JOURNAL OF GEOPHYSICAL RESEARCH, VOL. 106, NO. A4, PAGES 5661–5681, APRIL 1, 2001

# Evolution and dissipation of imbedded rotational discontinuities and Alfvén waves in nonuniform plasma and the resultant proton heating

Bernard J. Vasquez and Joseph V. Hollweg

Space Science Center, Institute for the Study of Earth, Oceans, and Space, University of New Hampshire, Durham

**Abstract.** We show that nonuniform Alfvén speed gradients across field lines generally arise from the evolution of Alfvén waves. The evolution of a group of nonlinear Alfvén waves with the same sign of parallel wavenumber generate small-amplitude pressure-balanced structures (PBSs) which cause the speed variations. This always causes refraction. In most cases, the Alfvén waves also couple to magnetosonic waves and acquire a weak compressional component and can undergo resonant absorption or transfer, wherein wave energy can propagate across field lines. At large amplitudes the waves also generate imbedded rotational discontinuities (RDs). Some of these RDs can be dissipated owing to resonant transfer. This process could partly contribute to the observed decrease of solar wind RDs with increasing distance from the Sun. Resonant transfer also triggers a cascade due to steepening, which leads to sustained proton heating. The cascade produces oblique and large wavenumber waves which travel in different directions and have associated compressions. Protons interact with these by pitch angle scattering. They gain energy from second-order Fermi acceleration and from Landau and transit time damping. Oblique waves are inferred to be present in the dissipation range of Alfvénic fluctuations at 1 AU. We argue that the process of proton heating should proceed similarly to simulation results. We also propose a role for the wave imbedded RD in coronal heating through its formation in the chromosphere and its likely dissolution in the corona where wave amplitudes are very small.

## 1. Introduction

Locally, Alfvénic fluctuations in the solar wind tend to have nearly constant magnetic intensity $B$, imbedded abrupt rotations, called rotational discontinuities (RDs), and a small compressional component which tends to be anticorrelated with $B$. *Vasquez and Hollweg* [1996a, 1996b, 1998a, 1998b, 1999] have shown that these properties can be partly explained from the weakly nonlinear behavior of (shear) Alfvén waves using a small-amplitude expansion of the nonlinear MHD equations. When all Alfvén waves have the same sign of parallel wavenumber $k_{\|}$, they generate second-order driven waves with the speed of an Alfvén wave but the polarization of a fast wave. To second-order, the sum of the magnetic fields gives a constant $B$. Magnetosonic waves are also generated to satisfy initial conditions but can be damped in a warm plasma.

A more complete description of Alfvén wave and imbedded RD evolution requires the inclusion of the effects of ion wave dispersion and kinetics, as well as of large amplitude. This is accomplished using hybrid numerical simulations with protons treated as particles and electrons as a fluid. *Medvedev et al.* [1997] used numerical calculations of the kinetic nonlinear Schröedinger equation and independently showed the formation of RDs and the tendency toward constant $B$.

The imbedded RD is generated when an Alfvén wave steepens. Its width is typically ~10 ion inertial lengths. Wave steepening gives the most natural explanation of why solar wind RDs are associated with Alfvénic fluctuations [e.g., *Riley et al.*, 1996]. The RD is not a separate entity, such as a soliton, but rather it is the continuation of the Alfvén wave down to scales where ion wave dispersion and kinetics determine the structure. As such, the RD and wave are physically inseparable.

The widespread presence and frequent observation of RDs in the solar wind are most readily explained if they are stable against dispersion. *Vasquez and Hollweg* [1998b] demonstrated that the wave imbedded RD is stable against dispersion, whereas previous studies [e.g., *Richter and Scholer*, 1989; *Vasquez and Cargill*, 1993] showed that isolated RDs can be unstable for parameters relevant to the solar wind [e.g., *Neugebauer*,



Paper number 2000JA000268.
0148-0227/01/2000JA000268$09.00

1989]. The principal difference between isolated and imbedded RDs concerns the presence of critical points in the former. A critical point occurs where all field and plasma spatial derivatives vanish. Isolated RDs have critical points in the upstream and downstream states. *Hau and Sonnerup* [1991] show from a critical point analysis of differential equations that waves cannot phase stand at RDs for most parameters and so the RDs are not stable. Waves with imbedded RDs have no critical points because there is no point in the wave where all derivatives vanish.

The presence of RDs in Alfvénic fluctuations can impose constraints on the evolution of the fluctuations as a whole. First, RDs provide a constraint on the role of the ponderomotive force $-\nabla B^2/8\pi$, which governs steepening in a compressible plasma. *Cohen and Kulsrud* [1974] were the first to show that there is sufficient time for Alfvén waves to steepen and form RDs near the Sun. If solar wind RDs are produced by wave steepening, then some phase coherence of the Alfvénic fluctuations must have existed at some point closer to the Sun, despite the overall phase incoherence which generally characterizes the observed fluctuations. Second, we will show in this paper that the evolution of RDs with distance from the Sun is influenced by nonuniformities in the medium through which they propagate. Thus their evolution can provide information about this medium.

For Alfvén waves propagating in many different directions it is very likely that some will couple to produce nonlinear forces in the perpendicular direction. *Vasquez and Hollweg* [1999] showed that the driven MHD solutions change in this direction because Alfvén waves do not propagate. Instead, a driven second-order fluctuation of the parallel magnetic field and density is generated. This causes the Alfvén speed to vary across field lines. Its effects are the main focus of this paper.

Even when all Alfvén waves have the same sign of $k_\parallel$, surprisingly complicated dynamics result due to the nonuniformities which are produced nonlinearly by the waves themselves. We find that imbedded RDs can evolve and dissipate. A cascade is initiated, which leads to sustained proton heating. This provides insight to the small-scale processes or microphysics which accompany a cascade. This microphysics concerns the individual motions of protons which ultimately dissipate the energy of the cascade. We intend to use our simulation results to explain some of the microphysics which we believe would arise in the interplanetary dissipation range based on corresponding properties of the simulated cascade.

The cascade which is produced in our simulations is rather special compared to others and has some properties with which the comparison to the interplanetary Alfvénic fluctuations can be partly made. The simulated cascade is a sustained one and has waves traveling in different and oblique directions. These are all qualitative observed or inferred properties of interplanetary Alfvénic fluctuations.

A well-studied area with applicable results on the microphysics associated with cascades concerns wave decay instability. This instability has some of the required features in that the cascade is sustained and has waves traveling in opposite directions (but along $\mathbf{B}_0$) [e.g., *Terasawa et al.*, 1986; *Machida et al.*, 1987; *Inhester*, 1990; *Vasquez*, 1995]. *Terasawa et al.* [1986] and *Machida et al.* [1987] examined a number of interactions between particles and large-amplitude waves which are similar to ones which arise in our simulations.

*Machida et al.* [1987] also make a detailed study of wave-particle interactions when wave trains are modulationally unstable and compare results with calculations using the derivative nonlinear Schröedinger (DNLS) equation. The wave trains undergo steepening, and in this sense, the results are applicable to our study. However, the cascade which develops involves waves traveling mostly in one direction.

The study of Alfvén waves in smoothly varying fields and plasma has been investigated numerically by many authors [e.g., *Sakurai et al.*, 1991; *Goossens et al.*, 1995; *Murawski et al.*, 1996; *Ofman and Davila*, 1997; *Ghosh et al.*, 1998; *Goldstein et al.*, 1999]. A difference between this paper and the cited studies is that the nonuniform plasma arises self-consistently from waves and so is not included initially. Furthermore, the cited studies treat one-fluid MHD which is not able to describe the internal structure of RDs and their interactions with protons.

We will show from the expansion of the MHD equations to higher orders that the equations become secular due to the second-order pressure-balanced structures (PBSs), which are produced by the first-order waves. These equations can be analyzed and reduced to a form corresponding to those of *Hollweg and Yang* [1988], which describes linear MHD wave evolution in a nonuniform plasma. From this basis a number of results can be applied which are well understood concerning Alfvén waves in nonuniform plasma [e.g., *Uberoi*, 1972; *Hasegawa and Uberoi*, 1982; *Lee and Roberts*, 1986] and kinetic Alfvén waves (KAWs) [e.g., *Lysak and Lotko*, 1996; *Gekelman et al.*, 1997; *Hollweg*, 1999]. However, when amplitudes are large, we will show that a number of significant departures from the small-amplitude theory occur.

Our analysis justifies the important emphasis given to nonuniformities in the sonic Mach number (ratio of fluctuation velocity to sound speed) expansions undertaken in *Bhattacharjee et al.* [1998, 1999]. They show that nonuniformities can explain the linear dependence of solar wind density fluctuations on the sonic Mach number.

The outline of the paper is as follows: Section 2 presents a synopsis of an analysis of the MHD equations extended to higher orders in wave amplitude. In section 3, simulations of Alfvén waves and imbedded RDs are presented. In one study, small-amplitude waves are evolved in an imposed nonuniform background. In other

studies, large-amplitude waves self-consistently generate a nonuniform background due to PBSs. In section 4, we discuss how generated PBSs might influence solar wind RDs and proton heating. We also discuss how RDs might form in the chromosphere and have a role in coronal heating. Section 5 summarizes our findings and gives our conclusions.

## 2. Higher-Order Analysis of the MHD Equations

We have carried out an expansion of the MHD equations to beyond second order. The algebra becomes lengthy, and so here we will cite the results and discuss some solutions which clarify the physics. The details are provided in Appendix A.

At zeroth order we take uniform background magnetic field $\mathbf{B}_0$ and density $\rho_0$, where the subscript denotes the order. At first order we include obliquely propagating linearly polarized Alfvén waves. Detailed second-order solutions are given by *Vasquez and Hollweg* [1999] (their section 2.3) by (26)-(28). When all the first-order Alfvén waves have the same sign of $k_\parallel$, then their generalized Reynolds stresses to second-order $\mathbf{R}_2 = (\mathbf{B}_1 \cdot \nabla)\mathbf{B}_1/4\pi - \rho_0(\mathbf{V}_1 \cdot \nabla)\mathbf{V}_1$ vanish. The only nonlinear force which governs evolution is $-\nabla B_1^2/8\pi$, and this enters the second-order equations as a known driver. The second-order equations are linear partial differential equations, and solutions can be expressed as a linear combination of Fourier components of $B_1^2$. Each Fourier component is associated with a distinct wave vector $\mathbf{k}$. The driven part of the solution consists of either (1) a propagating wave which cancels variations of $B$ to second order when $\mathbf{k}$ is oblique but not perpendicular (section 2.1) or (2) a second-order PBS which varies in the perpendicular direction (section 2.2). For nearly parallel propagation these solutions are not accurate, and waves can steepen. Magnetosonic waves are also produced as homogeneous solutions. Here we will focus mostly on the driven solutions since these do not damp away. In some instances the magnetosonic waves are important, and those cases will be considered in section 2.3.

### 2.1. Constant |B|

Higher-order interactions between Alfvén waves continue to have $\mathbf{R} = 0$. (Note that at each order we neglect any interactions between lower-order magnetosonic waves and Alfvén or driven waves.) The driving force comes only from $-\nabla B^2/8\pi$, and the form and solutions of the equations correspond to the ones obtained at second order. The value of $B^2$ can be expanded out to fourth order as

$$\begin{aligned} B^2 &= B_0^2 \\ &+ B_1^2 + 2\mathbf{B}_0 \cdot \mathbf{B}_2 \\ &+ 2\mathbf{B}_1 \cdot \mathbf{B}_2 + 2\mathbf{B}_0 \cdot \mathbf{B}_3 \\ &+ 2\mathbf{B}_1 \cdot \mathbf{B}_3 + B_2^2 + 2\mathbf{B}_0 \cdot \mathbf{B}_4 + \cdots . \end{aligned} \quad (1)$$

From second order and higher the rightmost term on each line of (1) is a homogeneous term involving the parallel component of $\mathbf{B}$ to the given order. The other terms are drivers which are products of two lower-order values of $\mathbf{B}$, and their sum at an order $\eta$ is denoted as $\mathrm{D}_\eta$. The nature of the driven solutions is to make $B$ constant. The solution which does this can be immediately obtained from (1) by having the homogeneous term for order $\eta$ cancel the part of $\mathrm{D}_\eta$ which varies in space. This gives

$$B_{\eta\parallel} = -(\mathrm{D}_\eta - \langle \mathrm{D}_\eta \rangle)/2B_0, \quad (2)$$

for $\eta \geq 2$ where $\langle \mathrm{D}_\eta \rangle$ is the space average of $\mathrm{D}_\eta$. The other components of $\mathbf{B}_\eta$ are obtained from $\nabla \cdot \mathbf{B}_\eta = 0$. The velocity fluctuations are the same as required for an Alfvén wave, and there are no density fluctuations. Thus these wave interactions lead to a truly constant-$B$ Alfvén waveform when the magnetosonic waves are damped. For a single Alfvén wave our series solution agrees with an exact constant-$B$ solution obtained by *Barnes and Hollweg* [1974] (see Appendix A for details).

In the parallel or nearly parallel direction, small-amplitude behavior changes and the underlying equations become secular. This is due to the steepening of the wave. Simulations of *Vasquez and Hollweg* [1998b] show that this wave steepening generates field-aligned or nearly field-aligned RDs. A constant $B$ and steady waveform results generally for waves with initial polarizations tending toward arc or spherical.

### 2.2. PBSs and Waves

*Vasquez and Hollweg* [1999] showed that second-order PBSs develop in directions perpendicular to $\mathbf{B}_0$. These have variations $B_{2\parallel}/B_0 = \rho_2/\rho_0$, and total pressure balance is satisfied to second order when $B_1^2/8\pi$ is included.

Equilibria beyond second order are prevented when interactions involve a PBS and a propagating wave. Equations describing this interaction are given by (A8)-(A10). First, we take the simpler case in which only refraction results. This occurs when the wave vectors of the first-order Alfvén waves are confined to a plane containing $\mathbf{B}_0$ and variations due to PBSs. We assume that $\mathbf{B}_0$ is in the $x$ direction and that a second-order PBS is generated with gradients in the $y$ direction. Alfvén waves confined to the $xy$ plane are then polarized along the $z$ axis. From (A8)-(A10), one can show that magnetic and velocity fluctuations in the $z$ direction become decoupled from components in the $xy$ plane. To third order, they are given by

$$\rho_0 \frac{\partial V_{3z}}{\partial t} - \frac{B_{0x}}{4\pi}\frac{\partial B_{3z}}{\partial x} = \frac{B_{2x}}{4\pi}\frac{\partial B_{1z}}{\partial x} - \rho_2 \frac{\partial V_{1z}}{\partial t}, \quad (3)$$

$$\frac{\partial B_{3z}}{\partial t} - B_{0x}\frac{\partial V_{3z}}{\partial x} = B_{2x}\frac{\partial V_{1z}}{\partial x}. \quad (4)$$

The left-hand sides of (3) and (4) describe the Alfvén wave; driver terms appear on the right-hand sides.

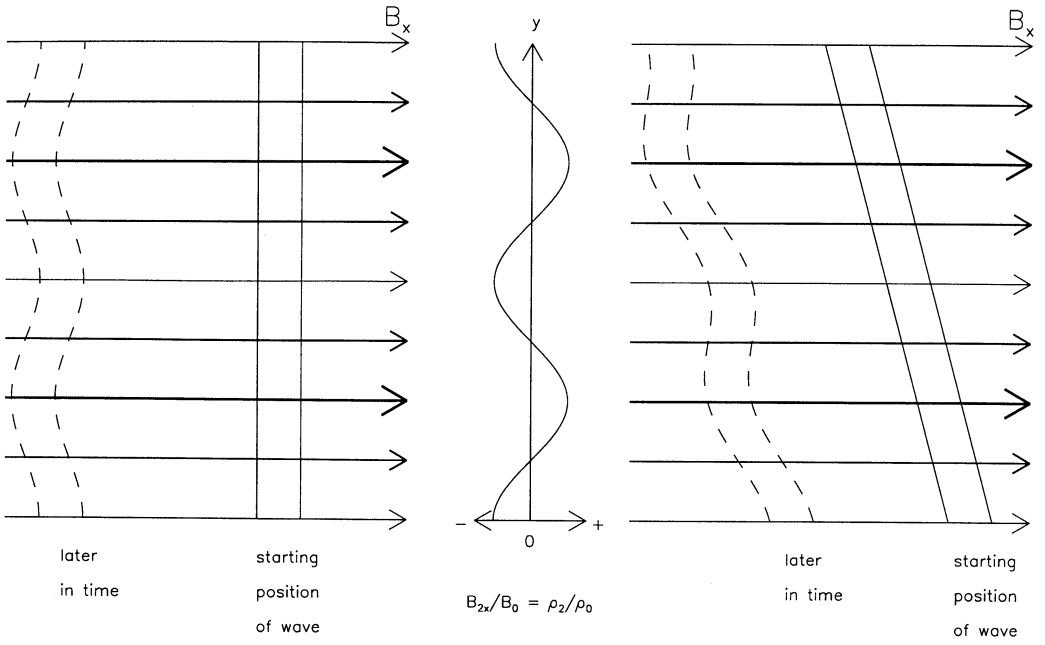


**Figure 1.** Schematic shows how a generated pressure-balanced structure (PBS) causes refraction of a wave with its normal initially along the (left) magnetic field and (right) oblique. Solid horizontal lines represent the time constant magnetic field in the $x$ direction. Thicker lines correspond to stronger fields. On the right-hand side is a plot of the change in $B_x$ and $\rho$ due to the PBS along the $y$ direction. These quantities are correlated and so are variations of the Alfvén speed. Lines across the magnetic field represent lines of constant phase for a wave. Adjacent solid and straight lines represent a plane wave at two distinct phases which is at its starting position. After some time, the wave moves to the left and is deformed by refraction. This is shown by two dashed lines. The wave on stronger lines of magnetic field outruns itself on weaker lines. Because of the sinusoidal variation of the speed in the $y$ direction, the lines are distorted into an approximate triangular form. The distance between the two lines remains a constant along the magnetic field. As a result, the perpendicular wavenumber varies, but the parallel wavenumber is unchanged.

These contribute to the tension of the magnetic field lines and so can alter the Alfvén speed. Equations (3) and (4) can be combined into one for $B_{3z}$

$$\frac{\partial^2 B_{3z}}{\partial t^2} - \frac{B_{0x}^2}{4\pi\rho_0}\frac{\partial^2 B_{3z}}{\partial x^2} = \frac{B_{0x}B_{2x}}{4\pi\rho_0}\frac{\partial^2 B_{1z}}{\partial x^2}. \quad (5)$$

Equation (5) shows that when a PBS and Alfvén wave interact, the sum and difference of their **k** values and wave frequencies $\omega$ is another Alfvén wave since the PBS has $k_x = 0$ and $\omega = 0$. The homogeneous solution of this equation gives the same frequency as that of the driver. Therefore solutions to (5) become secular, and the power series in wave amplitude will not converge uniformly.

A multiple-timescale expansion can resolve the secularity. We have written (5) in a manner where this can be applied without introducing new symbols for the stretched coordinates in space and time, but we must drop the subscript ordering in (5) and simply solve for $B_z$. Note in (5) that $B_{2x}$ is independent of $x$ and $t$, and so a Fourier transform can be applied in these dimensions. This leaves us with an inhomogeneous linear equation for $B_z$ whose dispersion relation can be shown to be

$$\omega^2/k_x^2 = B_{0x}^2(1 + B_{2x}/B_{0x})/(4\pi\rho_0). \quad (6)$$

This is equivalent to the second-order variation of $c_A^2$ that one would obtain if $c_A^2$ in the presence of a PBS is calculated directly from $c_A^2 = (B_{0x} + B_{2x})^2/(4\pi(\rho_0 + \rho_2))$. Thus the wave must refract.

**2.2.1. Effects of refraction.** From (6) the Alfvén wave propagates most rapidly along field lines where $B_{2x}$ is a maximum ($\omega/k = c_{A,max}$) and slowest where it is a minimum ($\omega/k = c_{A,min}$). Figure 1 illustrates how a wave refracts with a normal starting along the $x$ axis (left side) and in an oblique direction (right side). With time, lines of constant phase with normals initially along the $x$ axis turn more oblique between positions of the relative maxima and minima of $B_{2x}$. The parallel wavenumber remains unchanged, but the perpendicular one grows larger. When the normal is initially oblique, some become more aligned with the $x$ axis. If we treat the lines of phase as straight lines between each maximum and minimum of $B_{2x}$, then we can estimate how the local $k_y$ evolves between relative extrema as

$$k_y = k_{y0} + k_x \Delta c_A t/L, \quad (7)$$

where $k_{y0}$ is the initial value of $k_y$, $\Delta c_A = c_A(y_2) - c_A(y_1)$ is the difference between $c_A$ on two adjacent field

lines at positions $y_1$ and $y_2(> y_1)$ where the $c_A$ is a maximum or minimum, and $L = y_2 - y_1$. The quantity $\Delta c_A$ is positive when $y_1$ corresponds to a relative minimum and negative when $y_1$ corresponds a relative maximum. From (7), $|k_y|$ decreases wherever $k_x \Delta c_A < 0$ for $k_{y0} > 0$ or $k_x \Delta c_A > 0$ for $k_{y0} < 0$ until $t = T_{ca}$, the time of closest approach (denoted by subscript $ca$) to $\mathbf{B}_0$, when $k_y = 0$ given by

$$T_{ca} = -k_{y0} L / k_x \Delta c_A \tag{8}$$

and thereafter increases. Thus, for very large $t$ we expect $\mathbf{k}$ to tend strongly to oblique directions, but at intermediate times, $\mathbf{k}$ could be nearly field-aligned.

The outline of the phase lines in Figure 1 is very regular because only a single sinusoidal variation of $B_{2x}$ is present. In general, the outline would be very irregular, if many Alfvén waves combine to generate PBSs.

Because the wave has a $z$ polarization and is perpendicular to variations along $y$, the wave does not linearly couple with magnetosonic waves which are polarized in the $xy$ plane. Thus, while refracting, it remains a MHD Alfvén wave. This would only change if $k_\perp$ approaches the ion inertial scale $c/\omega_{pi}$ where the wave first becomes compressional [*Hollweg*, 1999] and the gyroradius scale. At these scales it becomes a kinetic Alfvén wave (KAW) with a small wave frequency $\omega \approx c_A k_\parallel$. Because the KAW is compressional, it has a parallel electric field component and can undergo Landau and transit time damping [e.g., *Lysak and Lotko*, 1996].

**2.2.2. Resonant transfer.** Generally, waves have components of $\mathbf{B}_1$ in the direction that $B_{2x}$ and $\rho_2$ varies. Refraction still takes place, but, the equations are not as easily solved because Alfvén and magnetosonic waves become coupled. In Appendix A, we show that the higher-order equations can be reordered into a more compact set which matches at lowest order the linear ones for a varying background plasma and magnetic field solved by *Hollweg and Yang* [1988]. The initial value of the Alfvén wave's frequency $\omega_0 = k_x B_{0x}/(4\pi\rho_0)^{1/2}$ would come to lie between a maximum $\omega_{A,max} = k_x c_{A,max}$ and minimum $\omega_{A,min} = k_x c_{A,min}$ once a PBS is generated. In these situations [e.g., *Uberoi*, 1972; *Hasegawa and Uberoi*, 1982; *Lee and Roberts*, 1986], waves can transport energy across field lines. Energy builds up along a resonant field line, via the process called resonance absorption or transfer. We will adopt the term resonant transfer to emphasize the propagation of energy. The resonant line from generated PBSs occurs where $B_{2x} = \rho_2 = 0$ so that the Alfvén wave frequency on this line equals $\omega_0$. Energy would be transported most rapidly away from lines where $\omega_A$ ($B_{2x}$ and $\rho_2$) attain extrema. As the energy increases on the resonant field line, $k_\perp$ grows larger, and the resonant wave resembles a surface wave. If this resonant wave reaches the perpendicular scales of $c/\omega_{pi}$ or the gyroradius, it could become a KAW.

The rate at which energy is transferred to a resonant field line can be estimated. Again, we take $\mathbf{B}_0$ in the $x$ direction and a PBS which varies in the $y$ direction. However, we now consider an Alfvén wave with a component of polarization in the direction that the PBS varies. Here we take the particular case in which the initial Alfvén wave propagates in the $xz$ plane and is polarized along the $y$ axis. A basic response of the wave is to refract, and this can be modeled by letting $B_y = A\cos[k_x x + k_z z - \omega(y)t]$ and having its frequency vary with $y$. (Note that since $k_y = 0$ initially, we have the situation shown on the left side of Figure 1 except that the wave vector has a component outside the plane of the figure.) This wave will couple with one in the $xz$ plane. With time, the dominant magnetic component on resonant field lines will be in the $z$ direction and perpendicular to $\mathbf{B}_0$. The converted wave is only weakly compressive and satisfies $\partial B_y/\partial y + \partial B_z/\partial z = 0$ to leading order. We can then estimate $B_z$ to be

$$B_z = -\frac{B_y}{k_z}\frac{d\omega}{dy}t. \tag{9}$$

We can approximate the time $T_{rt}$ of resonant transfer (denoted by subscript $rt$) from (9) to be when the magnetic energy in the $z$ component averaged over space is one half of that in the $y$ component, which gives

$$T_{rt} \approx \frac{|k_z| L}{2|k_x \Delta c_A|}, \tag{10}$$

where $d\omega/dy \approx |k_x|\Delta c_A/L$. The increase of $k_y$ for the forming wave around a resonant field line can be calculated from (7).

If the above Alfvén wave initially has finite $k_y$ evolution can be more complicated. In this case, the wave has first-order magnetic components in both the $y$ and $z$ directions. In regions where refraction causes the local value of $k_y$ to increase, the wave will immediately undergo the resonant transfer, as above. However, adjacent regions where $k_y$ decreases initially will have the wave energy increasing in the $y$ component without any transport of energy to the resonant field line. Transfer will be delayed until $t = T_{ca}$.

When resonant transfer occurs, one would expect to see an asymptotic state where wave energy is concentrated on resonant field lines and in the $z$ direction. This result would be most clearly seen if there were only one wave propagating in a nonuniform medium. However, it requires the interaction of two or more Alfvén waves to produce the nonuniform medium, and this complicates the resultant waveform. Evolution of the waveform then is tied to the polarization directions of the individual Alfvén waves. Those waves polarized in the $z$ direction would remain body waves with equal wave energy on all field lines. Only those with polarizations which include a $y$ component could undergo mode conversion.

### 2.3. Magnetosonic Waves

**2.3.1. Slow waves.** If forces produce fluctuations which are almost but not exactly in the perpendicular

direction, the waveform may still be modified by refraction. Here a slow wave is produced which would mimic a PBS [e.g., *Parenti et al.*, 1997; *Vasquez and Hollweg*, 1999]. Because its frequency is very small, a long time may pass before it is damped in a plasma. As a result, Alfvén waves could be refracted until the slow wave is damped.

**2.3.2. Fast waves.** In the work of *Vasquez and Hollweg* [1999], fast magnetosonic waves are shown to be produced in the perpendicular direction which cannot be Landau or transit time damped away. However, these are propagating waves, and the equations do not become secular. Their fluctuations along any field line would oscillate with time and would cancel out any net displacement of the Alfvén wave as compared to other field lines. Thus, in a time-average sense, no refraction would occur.

## 3. Simulation Results

We will examine the influence of generated PBSs on the evolution of Alfvén waves using $2\frac{1}{2}$-D hybrid simulations. The initial waves are given a wavelength of $\sim 251 c/\omega_{pi}$ (wavenumber $kc/\omega_{pi} = 0.025$), although Alfvénic fluctuations are actually 1-2 orders of magnitude longer. At this wavelength, waves are long enough to be relatively dispersionless, as is true in the solar wind, but small enough so that simulations can still feasibly compute ion gyromotion over several wave periods. Initially, $\delta\mathbf{B}$ for each wave is linearly polarized, and $\delta\mathbf{V} = \text{sign}(k_{\|}) c_A \delta\mathbf{B}/B_0$ is specified, as is appropriate for a MHD Alfvén wave.

The simulation results to be shown are performed on $128 \times 128$ grids in the $xy$ plane with cell sizes of $1.96 c/\omega_{pi}$. Positions will be normalized to $c/\omega_{pi}$ and wavenumbers to $(c/\omega_{pi})^{-1}$. Eighty protons per cell are distributed according to a drifting Maxwellian using a drift velocity equal to $\delta\mathbf{V}$. Ion temperatures $T_{0\|} = T_{0\perp}$ with respect to $\mathbf{B}_0$ are expressed as energy densities normalized to $\rho_0 c_A^2$. The ion beta (ratio of gas to magnetic pressure) is twice the value of the normalized temperature. Ion and electron temperatures are initially equal, and the electrons are treated as a massless, quasi-neutralizing fluid with a specific heat ratio of one. Time steps are 0.05 proton gyrocycles or $0.05\Omega^{-1}$. Time will be normalized to $\Omega^{-1}$.

Section 3.1 examines evolution when $\mathbf{B}_0$ is in the plane of the simulation, where only refraction is expected. We revisit a case of nonequilibrium which was not properly explained by *Vasquez and Hollweg* [1998b]. In section 3.2, evolution when $\mathbf{B}_0$ is out of the plane is examined where resonant transfer can occur.

### 3.1. $\mathbf{B}_0$ in the Simulation Plane

Most of the simulations undertaken in the work of *Vasquez and Hollweg* [1998b] showed that nearly constant-$B$ waves evolved and appeared to represent equilibria or steady propagating waveforms. However, they did find particular cases, which independent of RD development, did not give an equilibrium. Nonequilibrium occurred when a pair of Alfvén waves had wave vectors symmetrically positioned to either side of $\mathbf{B}_0$ so that $k_{\|,1} = k_{\|,2}$ and $k_{\perp,1} = -k_{\perp,2}$, where subscripts 1 and 2 refer to individual waves and $k_\perp$ is the perpendicular wavenumber.

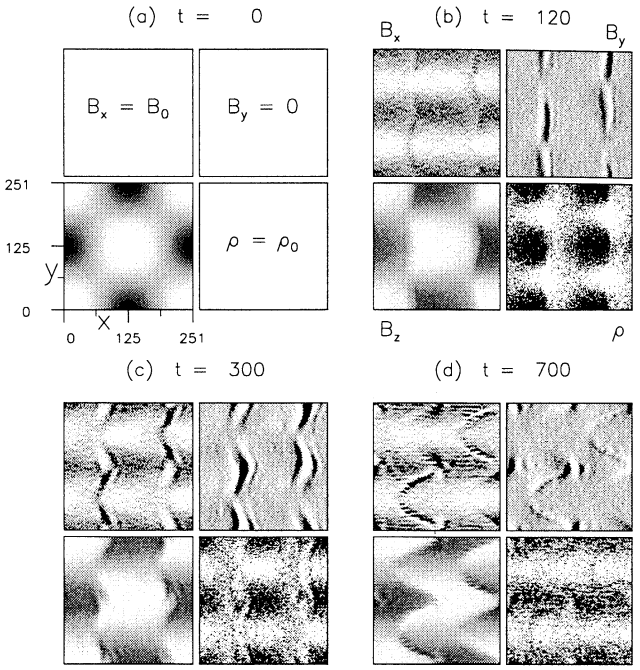


**Figure 2.** Evolution of a pair of Alfvén waves with wave vectors situated on opposite sides of $\mathbf{B}_0 = B_0\hat{\mathbf{x}}$ at equal oblique angles. Intensity plots are given as functions of position for $B_x$ (top left), $B_y$ (top right), $B_z$ (bottom left), and $\rho$ (bottom right) at (a) $t = 0$, (b) $t = 120$, (c) $t = 300$, and (d) $t = 700$. The intensity range normalized to $B_0$ for $B_x$ is 0.85–1.15, for $B_y$ is −0.2–0.2, for $B_z$ is −1.0–1.0, and for $\rho$ is 0.9–1.1 with light shades representing maximum values and dark shades minimum values. Coordinate axes are shown only for the plot of $B_z$ at $t = 0$ but apply equally for all plots. The plotted quantities are shown in a frame which moves to the left at the background Alfvén speed.

A simulation example is shown in Figures 2a-2d, where the $x$ axis is parallel to $\mathbf{B}_0 = B_{0x}\hat{\mathbf{x}}$ and the $y$ axis is perpendicular. The Alfvén waves are polarized along the $z$ direction. The amplitude of each wave is $0.5B_0$. The superposition of these two waves gives a maximum total amplitude of $B_0$. The initial ion temperature has $T_{0\|} = T_{0\perp} = 0.33$. Both waves have $k_\| = -0.025$, one has $k_\perp = 0.025$ and the other has $k_\perp = -0.025$. Unlike in the work of *Vasquez and Hollweg* [1998b, Figures 4a-4d], we do not include second-order fields initially and instead allow them to develop on their own. The second-order solution used in the perpendicular direction by *Vasquez and Hollweg* [1998b, p. 355] is incorrect in that they did not specify a variation in $\rho$.

Figures 2a-2d show intensity plots of $B_\|$ (top left), $B_y$ (top right), $B_z$ (bottom left), and $\rho$ (bottom right) for (a) $t = 0$, (b) $t = 120$, (c) $t = 300$, and (d) $t = 700$.

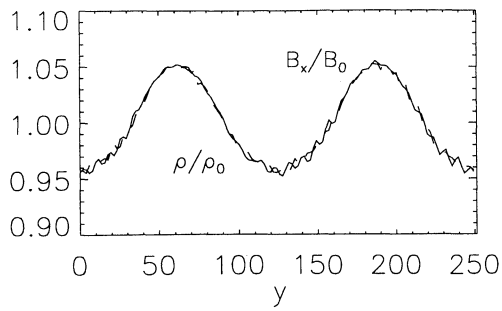


**Figure 3.** Plot of the average values of $B_x$ and $\rho$ in the $y$ direction at $t = 300$.

The plot is made in a frame moving at the Alfvén speed (based on $B_0/(4\pi\rho_0)^{1/2}$) to the left and parallel to $\mathbf{B}_0$.

As a group, the initial Alfvén waveform propagates in the $-x$ direction and steepens significantly within approximately $50\Omega^{-1}$ and begins to develop RD structure with normals along $x$. The transverse extent of these RDs reach a maximum by $t = 120$. Individual RDs can be seen lined up along vertical lines separated by horizontal lines where $B_z = 0$ at $t = 120$ (Figure 2b). These RDs generate ion cyclotron waves from their layers which cause dispersive spreading of the layers. This is an additional source of nonequilibrium that *Vasquez and Hollweg* [1998b] show is function of the initial wave polarization.

With time, adjacent RDs continually turn their normals oblique, and neighboring RDs do this in opposite senses (i.e., one toward $+\hat{\mathbf{y}}$ and the other toward $-\hat{\mathbf{y}}$). To maintain $\nabla \cdot \mathbf{B} = 0$, the RD acquires a field component in the $x$ direction. Thus the diminishment of the RD layers in plots of $B_y$ should not be taken as a diminishment of the RD overall. The turning of the normals is continuous, and no equilibrium is obtained.

The turning of normals is ultimately due to the difference of wave vectors which gives a Fourier component of the ponderomotive force in the perpendicular direction. This leads to a PBS and perpendicular fast waves of two cycles in the $y$ direction. (In the work of *Vasquez and Hollweg* [1998b], a true PBS does not develop because of the incorrect starting conditions which resulted in a smaller gas pressure than needed to balanced the imposed magnetic pressure.) Figure 3 shows the plot of $B_x/B_0$ (solid line) and $\rho/\rho_0$ (dashed line) as a function of $y$ averaged for all $x$ and $t$. The time average removes the perpendicular fast waves, so that the PBS alone is plotted. Across $y$, this PBS has $B_x/B_0$ and $\rho/\rho_0$ nearly equal with an amplitude of 0.05. Its shape differs only a little from a sinusoid. The expected speed difference is $0.025\, c_A$ based on (6). The actual amount of refraction is greater due to the development of ion cyclotron waves which disperse from RDs and fall behind owing to their slower phase speeds. These waves have maximum amplitude along $y = 0$ and 125, where $c_A$ is a minimum. Thus the waveform along these $y$ travels slower than expected for a MHD Alfvén wave.

In these simulations, waves and RDs refract and as expected do not undergo resonant transfer. A quasi-steady RD never develops from this initial state and undergoes dispersive spreading due to ion cyclotron waves from the time of its formation. Since we expect RDs to be steady against dispersion, at least initially, in the solar wind, we will not pursue this case further in this paper.

### 3.2. $\mathbf{B}_0$ Out of the Simulation Plane

With hybrid simulations it is difficult to test directly the small-amplitude theory with respect to generated PBSs. For small-amplitude waves the gradients of wave speed which develop are small and their effects require long times to study. Hybrid simulations typically cannot maintain sufficient accuracy to follow evolution to the times needed. Moreover, small-amplitude PBSs can also be overwhelmed by density perturbations induced by particle noise.

This forces us to examine the evolution of large-amplitude waves where small-amplitude theory need not be valid. Indeed, we will find that there are very important differences. To show this contrast better, we first demonstrate that the simulations can recover the linear effects of a varying background on a small-amplitude wave by including a large background variation rather than attempting to generate one self consistently. Evolution will be compatible with the one in section 2.

Section 3.2.1 examines nearly linear wave evolution toward a KAW in the presence of the large background variation. Section 3.2.2 examines large-amplitude wave evolution when the PBSs are generated self-consistently.

**3.2.1. Small-amplitude wave in an initially varying background.** We consider the interaction of a first-order purely magnetic structure and an Alfvén wave using a $2\frac{1}{2}$-D simulation when $\mathbf{R}_2 \neq 0$ and $\mathbf{V}_1 \times \mathbf{B}_1 \neq 0$. In this case, we do not explain the origin of the structure, but by including it at an amplitude comparable to that of the Alfvén wave, we will drive this waveform through refraction quickly to a saturated state. This state will ultimately consist of a KAW with large $k_\perp$ but small $k_\parallel$ and $\omega$. Dissipation occurs via Landau and transit-time damping.

In the simulation, $\mathbf{B}_0$ lies at 45° to the simulation plane $xy$ so that all wave vectors in the simulation are oblique wherein only the $y$ axis is perpendicular to $\mathbf{B}_0$. The first-order structure has its wave vector in the $y$ direction, has magnetic but no kinetic energy, and has its magnetic field $B_p^s = 0.25 B_0 \cos(0.025y)$ ($s$ means structure and $p$ perpendicular) along $\hat{\mathbf{p}} = \hat{\mathbf{y}} \times \mathbf{B}_0$. The initial Alfvén wave has its wave vector in the $-x$ direction and its magnetic field $B_y = 0.25 B_0 \cos(-0.025x)$ along the $y$ direction. Figures 4a-4d are intensity plots of $B_\parallel$ (top left), $B_y$ (top right), $B_p$ (bottom left), and $B_p^w = B_p - B_p^s$ (bottom right) for (a) $t = 0$, (b) $t = 500$, (c) $t = 1000$, and (d) $t = 1500$. (Here $w$ means the component associated with the wave.) Initially, the fields of the wave and structure are perpendicular to one another

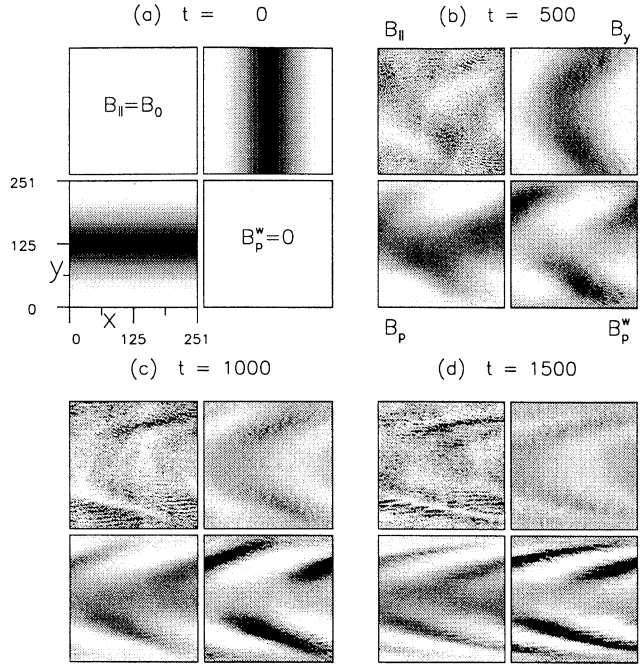


**Figure 4.** Simulation results of the interaction of a first-order Alfvén wave and magnetic structure with equal amplitudes of $0.25B_0$. Intensity plots are given as functions of position for $B_{||}$ (top left), $B_y$ (top right), $B_p$ (bottom left), and $B_p^w$ (bottom right) at (a) $t = 0$, (b) $t = 500$, (c) $t = 1000$, and (d) $t = 1500$. The intensity range normalized to $B_0$ for $B_{||}$ is 0.9–1.1, for $B_y$ and $B_p^w$ is −0.25–0.25, and for $B_p$ is −0.25–0.25 at $t = 0$, −0.375–0.375 at $t = 500$, and −0.5–0.5 at $t = 1000$ and 1500. $\mathbf{B}_0$ lies outside the simulation plane so that the generalized Reynolds stress $\mathbf{R}$ is nonzero. The wave is initially polarized in the $y$ direction, and the structure is in the $p$ direction. Both have equal magnetic energy, but the structure has no kinetic energy. The wave refracts and $B_p^w$ increases on resonant field lines.

and so in Figure 5a are seen separately in plots of $B_y$ and $B_z$, respectively. The density is uniform initially, and $T_{0||} = T_{0\perp} = 0.083$.

In Figures 4b-4d, $B_y$ is noticeably bowed to the left because the Alfvén phase speed varies along the $y$ axis, due to the additional magnetic field of $B_p^s$. The phase speed can be shown to be

$$\omega/k_x = c_A(\cos 45° - \sin 45° \frac{B_p^s(y)}{B_0}). \qquad (11)$$

As it refracts, the wave develops gradients in the $y$ direction and must satisfy $\partial B_y/\partial y = -\partial B_p/\partial x$. At the same time, the magnetic structure evolves second-order variations in $B_{||}$ and $\rho$ which cause it to develop into a nearly time constant PBS. Since $B_p^s$ is nearly time constant, the energy of the refracting wave ends up in $B_p^w$ and is concentrated at $y = 64$ and $y = 180$, which are the resonant field lines (i.e., $B_p^s = 0$). By $t = 1500$ a resonant wave develops with an unchanged $k_{||} = 0.025$ but $k_\perp = 0.2$ and width of $30c/\omega_{pi}$. The perpendicular scales will eventually become small enough that ion inertial length and gyroradius effects become significant, and then the resonant wave will be a KAW.

Figure 5a plots the wave energy normalized to the initial amplitude squared ($0.25^2B_0^2$) in $B_y$ (solid line) and $B_p^w$ (dashed line) as a function of time. In the simulation, energy is nearly exchanged between $B_y$ and $B_p^w$ with an approximate 12% loss due mainly to the development of compressions and to Laudau damping. Energy saturates in $B_p^w$ after $t = 600$. In this state, the wave magnetic field becomes more aligned in the $p$ direction and in the same direction as the structure. Figure 5b plots the value of the Alfvén ratio (which is ratio of fluctuation kinetic to magnetic energy) as a function of time. The ratio oscillates around the initial value of 0.5 and then saturates near 0.5, for $t > 600$. This shows that only the excess magnetic energy in structures determines how far the Alfvén ratio is reduced below one in the saturated state. The developing KAW closely approximates a MHD Alfvén wave.

The wave evolution in this case is consistent with what is expected from our analysis. We believe it is very likely that small-amplitude waves which self-consistently generate PBSs will behave in a similar manner and consistent with theory.

**3.2.2. Large-amplitude wave evolution with generated PBSs.** We examine the evolution of a pair Alfvén waves configured in the simulation plane as they are in Figures 2a-2d. The direction of $\mathbf{B}_0$ is 22.5° outside the simulation plane and in the $xz$ plane. The initial density is uniform, and $T_{0||} = T_{0\perp} = 0.083$. The

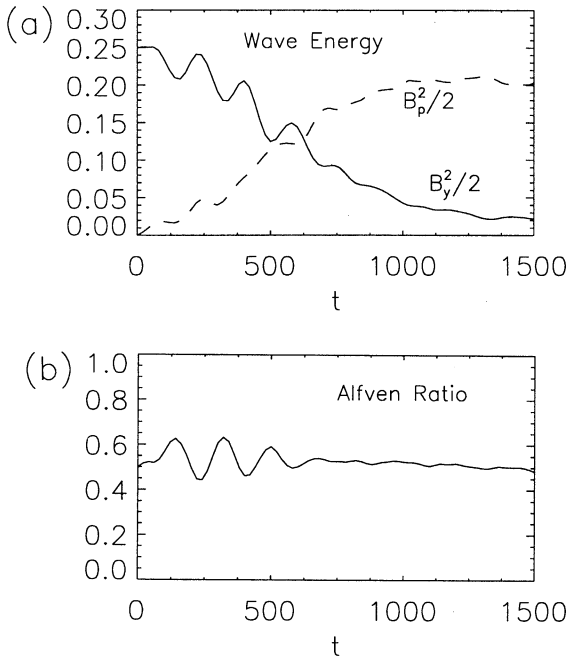


**Figure 5.** Plot of (a) the wave magnetic energy in the $y$ and $p$ directions and (b) the Alfvén ratio $r_A$ as a function of time for the case given in Figure 4. At long times, wave energy is nearly exchanged between the $y$ and $p$ components, and $r_A$ returns nearly to its starting value.

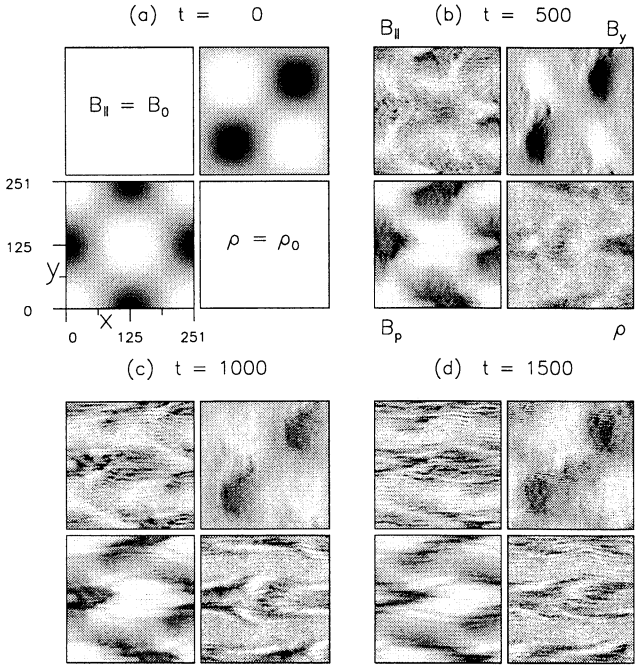


**Figure 6.** Simulation results of the interaction of a pair of first-order Alfvén waves with equal amplitudes of $0.5B_0$. Intensity plots are given as functions of position for $B_\parallel$ (top left), $B_y$ (top right), $B_p$ (bottom left), and $\rho$ (bottom right) at (a) $t = 0$, (b) $t = 500$, (c) $t = 1000$, and (d) $t = 1500$. The intensity range normalized to $B_0$ for $B_\parallel$ is 0.75–1.25, for $B_y$ is −0.3–0.3 at $t = 0$ and 1500 and is −0.5–0.5 at $t = 500$ and 1000, for $B_p$ is −0.9–0.9, and for $\rho$ is 0.6–1.4 $\mathbf{B}_0$ lies outside the simulation plane. PBSs develop leading to refraction, resonant transfer, and dissipation of waves and imbedded RDs.

Alfvén waves each have an amplitude of $0.5B_0$, and their vector addition gives a maximum total amplitude of $0.93B_0$. For this case, Figures 6a-6d give intensity plots of $B_\parallel$ (top left), $B_y$ (top right), $B_p$ (bottom left), and $\rho$ (bottom right) for (a) $t = 0$, (b) $t = 500$, (c) $t = 1000$, and (d) $t = 1500$. The plot is in a frame moving to the left at $0.92c_{A0}$.

As expected, the waves generate a PBS in the $y$ direction with two cycles. Along $y = 0$ and 125, $B_\parallel/B_0$ and $\rho/\rho_0$ attain minimum values (= 0.94) for the PBS and along $y = 63$ and $y = 188$ have maximum values (= 1.06). This causes refraction and resonant transfer. Refraction can be seen in the turning of phase fronts to more oblique angles beyond $t = 500$. By $t = 1500$ the fronts have turned well into the perpendicular direction. The simulation is approaching its limit of accuracy and is halted.

Some wave energy is expected to be transferred across field lines toward resonant ones at $y = 31$, 94, 157, and 220 where $\delta\rho = \delta B_\parallel = 0$. The full effects of transfer are delayed until after $t = T_{ca} = 500$ when all wave fronts turn oblique. The most affected regions occur where the wave is mostly polarized in the $y$ direction which is along $y = 63$ and $y = 176$. Here the average amplitude of $B_y$ decreases with time, while that of $B_p$ remains nearly constant. This is indicative of the effects of resonant transfer.

Generation of the PBS and the resultant refraction and resonant transfer are consistent with our expectations based on small-amplitudes theory. However, there are differences, too. First, there are additional compressions with substantial amplitude varying along field lines. They are especially large along $y = 0$ and 125 with deep minima of $\rho/\rho_0 = 0.7$. These originate from the coupling of Alfvén to magnetosonic waves. These introduce additional variations of the Alfvén speed and affect local wave vectors and normals.

Second, large-amplitude waves steepen and produce RDs. At $t = 500$ these can be seen as sharp changes in between minimum and maximum values in plots of $B_y$ along $y = 63$ and $y = 176$ and $B_p$ along $y = 0$ and 125. These have normals approximately in the $-x$ direction and occur two per wave cycle. Their widths are 20 $c/\omega_{pi}$.

Third, some RDs are dissipated while others remain intact. When wave energy in the $y$ direction is transferred away from waves and RDs along $y = 63$ and $y = 176$, these RDs are removed. The RDs along $y = 0$ and $y = 125$ and between resonant field lines are disrupted but remain intact. They undergo continual refraction and produce field and density fluctuations with large-$k_\parallel$ and -$k_\perp$ along their entire length. These fluctuations are mainly associated with fast waves and compressions. RD widths diminish as they turn into the perpendicular direction. However, they remain thicker than expected based simply on refraction of their normals from (7). We conclude that dispersion keeps layers relatively thick with widths of $10c/\omega_{pi}$ or more. (We have also followed this evolution on a 256 by 256 grid and find similar results to those shown in Figures 6a-6d.)

Fourth, wave energy does not build up to large values on the resonant field lines and KAWs are not produced. Instead, dissipation and heating are widespread. Figures 7a-7d shows intensity plots of $T_\parallel$ (left) and $T_\perp$ (right) as functions of position for (a) $t = 0$, (b) $t = 500$,

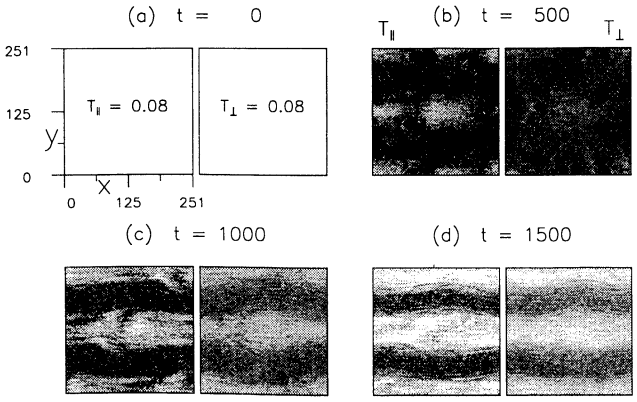


**Figure 7.** Intensity plots of (left) $T_\parallel$ and (right) $T_\perp$ as functions of position and time. Intensities range from 0.08 to 0.25 where darker shading corresponds to lower temperatures. Heating is widespread.

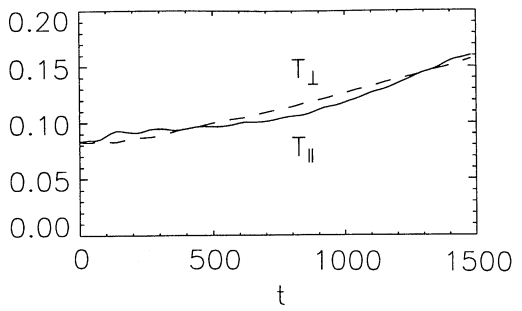


**Figure 8.** Plot of $T_{||}$ (solid line) and $T_{\perp}$ (dashed line) as functions of $t$. Temperatures nearly double.

(c) $t = 1000$, and (d) $t = 1500$. The components of temperature are calculated with respect to the local magnetic field and the corresponding thermal energy densities are normalized to $\rho_0 c_A^2 = B_0^2/4\pi$. Heating is mainly uniform and not confined to resonant field lines. Heating is seen in regions where wave energy has been mostly transferred away ($y = 63$ and 188). By $t = 1500$, protons are nearly 1.5 times hotter than initially and more in $T_{\perp}$ than $T_{||}$. Around $y = 0$ and 125, even more heating occurs because of the disruption of RDs. By $t = 1500$, protons here are nearly 2.5 times hotter than initially in both $T_{||}$ and $T_{\perp}$. Some particularly high and low temperatures are seen along the resonant field lines. Because of the large variations of $\rho$ on these lines, the variability is in part due to reversible compressional heating. The widespread occurrence of heating is due to the interaction of large-$k$ waves which originate in the vicinity of RDs and then spread away.

Figure 8 plots the average $T_{||}$ (solid line) and $T_{\perp}$ (dashed line) in the simulation box as a function of $t$. $T_{||}$ is greater than $T_{\perp}$ for $t \leq 400$. We believe this is a result of compressions which accompany steepening as the imbedded RDs are produced. Some heating from resonant transfer also occurs during these times. Starting around $t = 500$, there is a distinct increase in the rate of heating, when the full effects of resonant transfer occur and continue through $t = 1500$. Between $t = 500$ and 1500, each component of temperature increases by approximately 0.05 with corrections for the energy error (2% increase) in the simulations.

The wave magnetic field power spectrum develops an approximate $k^{-2}$ spectrum. This develops by $t = 100$. The spectral index remains relatively unchanged thereafter, although the wave power becomes more focused in oblique directions with time. We interpret this spectrum as a cascade due to wave steepening.

The simulation spectrum does not have the same slope as the inertial subrange of interplanetary Alfvénic fluctuations which on average has $k^{-5/3}$. The steeper form of the spectrum, especially because it involves oblique waves, can serve for a study of possible wave-particle behavior in the interplanetary dissipation range which on average has $k^{-3}$.

We conclude that the proton heating is sustained by a cascade driven by the ponderomotive force which gives steepening and the $k^{-2}$ spectrum. Resonantly transferred wave energy added to preexisting and large-amplitude waves causes gradients in the magnetic pressure to form. In the absence of the nonlinear ponderomotive force, waves simply become superposed on one another. In contrast, large-amplitude waves steepen in response to the total wave magnetic intensity which builds up and varies spatially. Wave energy transferred (mostly in $B_y$), as well as preexisting wave energy (mostly in $B_p$), is then cascaded to large $k$. Waves with large-$k$ originate in the vicinity of RDs and then spread away from RDs so as to affect a wide area. Ultimately, dissipation occurs and heats protons.

From the cascade, waves with large-$k$ travel in different oblique directions and have associated compressions. As a result, protons cannot remain resonant or correlated with a single wave for a long time. Following the trajectories of individual protons, we find little reflection or direct cyclotron acceleration. Instead, protons pitch angle scatter and diffuse in velocity space.

Protons gain energy first from second-order Fermi acceleration as they interact with many waves [e.g., *Terasawa et al.*, 1986; *Karimabadi et al.*, 1992]. A single resonant wave heats $T_{\perp}$ and tends to cool $T_{||}$. In the presence of additional waves moving in different directions, protons can random walk and so heat both $T_{||}$ and $T_{\perp}$ because they can resonate with one wave after another. A second source of heat comes from Landau and transit time damping the wave compressions. These interactions are likely to be aided by finite amplitude resonance broadening which can occur at relatively small amplitudes ($\delta B/B \gtrsim 10^{-3}$ [e.g., *Karimabadi et al.*, 1992]).

**3.2.3. Other cases.** We have run the simulation for a number of other parameters. Doubling all length scales reduces the rate of resonant transfer by one half and the heating of protons by about one half, as is expected.

At higher initial values of $T_0$ we find that the variation of Alfvén speed is nearly the same. This gives a similar rate of resonant transfer. The rate of heating is decreased somewhat. At $T_{0||} = 0.33$ we find a rate of 0.04 per $1000\Omega^{-1}$, which is 80% of that at $T_{0||} = 0.08$. This decrease is probably due to enhanced Landau damping of fast waves and compressions, which limits their amplitudes and so efficiency in transferring energy to protons.

When $\mathbf{B}_0$ is 45° above the simulation plane, the PBS has smaller amplitudes on average, and wave phase speeds are also smaller. Evolution occurs more slowly than in previous cases.

## 4. Discussion

In this section, we examine the possible influence of generated PBSs on Alfvénic fluctuations and imbedded RDs in the interplanetary medium. Their effects come primarily from the cross-field gradients of the Alfvén speed introduced by the PBSs which lead to refraction

and resonant transfer. Another type of nonuniformity is the velocity shear which is important in the solar wind but is not investigated here. Refraction and resonant transfer can also occur from the velocity shear [e.g., *Yang and Hollweg*, 1991; *Ghosh et al.*, 1998], but the shear can have additional effects concerning mode coupling [e.g., *Kaghashvili*, 1999] and turbulence [e.g., *Coleman*, 1968; *Goldstein et al.*, 1999].

We will treat an ideal situation in which the Alfvén waves are purely outgoing. In the interplanetary medium, most of the Alfvénic fluctuation flux is outgoing in high-speed streams. An ingoing component does evolve in the solar wind from partial reflection [e.g., *Matthaeus et al.*, 1999b] and nonlinearities [e.g., *Terasawa et al.*, 1986; *Machida et al.*, 1987]. This can generate quasi-2-D turbulence [e.g., *Oughton et al.*, 1994; *Matthaeus et al.*, 1996; *Spangler*, 1999] which affects many properties of the fluctuations. As such, our assumption of purely outgoing waves is unable to explain all features of Alfvénic fluctuations, especially with regards to the Alfvén ratio [e.g., *Goldstein et al.*, 1995] and power spectra. Yet, with this assumption, our results isolate physical processes which can then be compared to other situations in which the ingoing component and its effects are also examined.

In section 4.1, we estimate the time for refraction due to PBSs, and in section 4.2, the time of resonant transfer. Section 4.3 examines how refraction and resonant transfer can affect solar wind RDs, and section 4.4 discusses their influence on proton heating. In section 4.5, we discuss the production of KAWs.

### 4.1. Refraction Time

The timescale on which refraction strongly modifies a waveform can be estimated using (7). We define the refraction time $T_r$ as the time it takes for the plane wave to turn from 0° to 45° (i.e., $|\delta k_\perp/k_\parallel| = 1$), which is $T_r = L/|\Delta c_A|$.

At 1 AU the radial wavelength of Alfvénic fluctuations is typically $\approx 2 \times 10^6$ km. Assuming this is typical of the perpendicular wavelength, generated PBSs would have $L$ equal to a quarter of this wavelength or $L \approx 5 \times 10^5$ km. At 0.3 AU we would expect $L \approx 2 \times 10^5$ km based on spherical expansion. We also take $c_A \approx 150$ km/s and $\delta\rho/\rho_0 \approx 0.01$ so that $\Delta c_A$ is about 1.5 km/s. Then, $T_r \approx 37$ hours at 0.3 AU.

The estimate of $T_r$ uses an average scale. Alfvenic fluctuations exist over many scales, and we anticipate that PBSs would be generated on all corresponding scales in accord with the scale dependent and local average value of $\mathbf{B}_0$. The power spectrum of fluctuations in the energy containing range scales as $k^{-1}$, and as $k^{-5/3}$ in the inertial subrange. We expect that $\Delta c_A$ is proportional to the wave amplitude squared or wave power, and that $L$ is proportional to $k^{-1}$. Then, $T_r$ is proportional to a constant in the energy containing range, so that these scales refract at the same rate, and proportional to $k^{2/3}$ in the inertial range, so that the larger scales with their larger amplitudes refract faster.

Refracting at the estimated rate, purely outgoing Alfvén waves would be fairly steady over times small compared to the solar wind convection time. Only over the long convection times of transport from the Sun would refraction due to these generated PBSs become significant. In a solar wind moving at 500 km/s an outgoing wave propagating at 150 km/s would be transported a distance of 0.58 AU in 37 hours.

Spherical expansion would tend to align wave vectors in the radial direction. Gradients across field lines can oppose this. Wave vector directions cannot be obtained using WKB theory because the generated PBSs haves scales of order of the wavelength. Wave directions can be determined following the motion of planar surfaces between field lines [e.g., *Hollweg*, 1975; *Heinemann*, 1980].

For a purely radial magnetic field, distances between field lines vary as $r$. A wave surface at 0.3 AU aligned in the radial direction turns by 21° away from the radial direction due to perpendicular gradients when it reaches 1 AU. This assumes that the solar wind is moving at 500 km/s, average $c_A = 150(0.3/r)$ with $c_A$ in km/s and $r$ in AU, and that the PBSs have $L = 2 \times 10^5$ km at $r = 0.3$ AU and $\Delta c_A = 1.5$ km/s between 0.3 and 1 AU. (The value of $\Delta c_A$ can be assumed constant between 0.3 and 1 AU because smaller $c_A$ farther from the Sun is compensated by larger $\delta\rho/\rho$.) The rate of turning is about one half of that without expansion.

Starting at an oblique angle of 45°, expansion is faster and turns the wave surface to about 32° by 1 AU when the PBSs halts this motion. Greater amounts of refraction over expansion can be realized from perpendicular gradients of $c_A$ in the radial-azimuth plane when $\mathbf{B}_0$ spirals outward. Moreover, expansion can aid in turning wave normals oblique to $\mathbf{B}_0$. These effects arise because the distance between field lines increases less than $r$ when the field spirals outward.

The estimated refraction time is based on a straightforward arrangement of PBSs which vary exactly perpendicular to field lines for all $r$. Our treatment of the generation of PBSs among waves treats the initial plasma as uniform so that it could only be applied to a small region of the solar wind. Because the background varies with $r$ and waves relative to it, new PBSs could arise at larger $r$ which are arranged differently. Then PBSs would vary at least slowly in other directions. Additionally, large-amplitude waves can generate compressions along field lines. Even in the simulations of just two waves, some compressions occur along the field lines. Additionally, compressions could also arise from mixtures of forward and backward waves and from magnetosonic waves.

In this new situation, wave vectors would fluctuate in direction, in addition to their steadier refraction from PBSs in the perpendicular direction. In this respect, refraction into the perpendicular direction would be de-

layed. However, they could also increase the rate of refraction if the local value of $L$ at greater $r$ increases less than expected for geometric expansion. In this case, a planar surface at some $r_1$ would eventually be broken into smaller sections because it encounters PBSs arranged closer together on field lines. If $\Delta c_A$ remains nearly the same, the smaller sections would be easier to refract into the perpendicular direction.

In the solar wind a large number of waves propagate. These could generate variations of $c_A$ on so many scales and directions that the solar wind might be described as a random medium [e.g., *Valley*, 1974; *Malara et al.*, 1999]. A random walk of wave vectors would have them slowly wander into the perpendicular direction and so lengthen the refraction time. *Valley* [1974] has shown that Alfvén waves can scatter and couple to magnetosonic waves and that plane waves can lose coherence in random media.

### 4.2. Resonant-Transfer Time

Generally, Alfvén waves will have components of $\mathbf{B}_1$ and $\mathbf{V}_1$ in directions where generated PBSs vary. This causes not only refraction but also resonant transfer. The resonant transfer time $T_{rt}$ on which this occurs can be estimated using (10). For some representative parameters we let $k_z/k_x \sim 1$, $L = 2\times10^5$ km, $\Delta c_A = 1.5$ km/s, and we find that $T_{rt} = 19$ hours. The change in perpendicular wavenumber is given in (7) and evolves as does $T_r$.

The estimate is based on the time of turning from when the wave vector is closest to $\mathbf{B}_0$ and has increasing oblique angles. In section 4.1, expansion was found to reduce the turning rate from exactly perpendicular PBSs by about one half, and so a better estimate would have $T_{rt} = 38$ hours.

Not all waves will be turning more oblique at a given $r$, and not all will be polarized in a direction of significant variation. Thus resonant transfer cannot affect all waves on the same timescale at the same $r$.

Finally, we noted in section 4.1 that refraction was stronger in the radial-azimuthmal $r$-$\phi$ plane due to the spiraling of the interplanetary magnetic field. If resonant transfer also occurs, then there should be more fluctuation power in the $\hat{\theta}$ direction which is perpendicular to this plane and to $\mathbf{B_0}$. Near 1 AU, and in the ecliptic, magnetic fluctuation power anisotropies are observed. For instance, *Belcher and Davis* [1971] observed a 5:4 ratio between power in the $\hat{\mathbf{r}}\times\hat{\mathbf{B}}_0$ and $(\hat{\mathbf{r}}\times\hat{\mathbf{B}}_0)\times\hat{\mathbf{B}}_0$ direction. This is consistent with transfer but is not a large effect. So this could be evidence that transfer has little influence or the difference in refraction rates between the $r$-$\phi$ plane and other planes is small.

### 4.3. RD Evolution

Locally, Alfvénic fluctuations and imbedded RDs would appear to be approximately steady propagating waveforms. Yet, it is well known that over large distances in the solar wind, important changes occur [e.g., *Matthaeus and Goldstein*, 1982; *Bavassano et al.*, 1982; *Roberts et al.*, 1987a, 1987b]. One change is the decrease in the occurrence frequency of RDs observed with increasing distance $r$ from the Sun [e.g., *Behannon*, 1978; *Neubauer and Barnstoff*, 1981; *Mariani et al.*, 1983; *Lepping and Behannon*, 1986].

Approximately, 3 RDs per hour are seen near 0.3 AU and only 1 per hour near 1 AU. One least squares fit to the number of discontinuities which rotate fields gave a decreasing frequency proportional to $r^{-1.28\pm0.35}$ [*Behannon*, 1978], and most of this decrease is due to RDs. More RDs are observed in high-speed solar wind [e.g., *Neugebauer*, 1992]. Beyond 1 AU, *Tsurutani and Smith* [1979] and *Tsurutani and Ho* [1999] find that the observed numbers of RDs per hour continue to decrease.

How is this decrease to be explained if RDs are stable against dispersion? Observations of RDs are always conservative and so underestimate the actual number. For instance, RDs with normals nearly perpendicular to the spacecraft or field rotations less than a certain amount are not counted. These selection effects probably occur equally at all $r$. A selection effect which could spuriously give a decrease of RDs with $r$ can arise from biases toward narrow RD widths [e.g., *Tsurutani and Smith*, 1979; *Tsurutani and Ho*, 1999]. RD widths increase with $r$ and are proportional to the local thermal proton gyroradius or $c/\omega_{pi}$. However, within 1 AU, discontinuity widths are preferentially small [see *Lepping and Behannon*, 1986, Figure 11] so that few RDs would be lost in this way.

Through simulations, we have associated the evolution of RDs with propagation through a medium which varies across field lines. Outside of reconnection, the only other study of RDs in such nonuniform media is given by *Neubauer* [1976]. He treats the nonuniform solar wind as a set of uniform and contiguous flux tubes [e.g., *Hollweg*, 1982a]. The flux tubes are held in force balance by tangential discontinuities (TDs), which are static discontinuities with zero normal magnetic field. The interaction of RDs with TDs was determined using Reimann solutions of the MHD equations. The interactions can cause RDs to radiate MHD wave modes from where their edges are in contact with TDs. Over time, this can diminish the extent of the RD and cause plasma heating. Because this process is limited to the edges of the RD, the effects appear to be small.

In high-speed streams, TDs do not occur as frequently as RDs, especially near the Sun. Smooth and continuous variations, even between TDs, are more often observed so that models confining all gradients to discontinuities are not completely accurate.

Geometric effects in an expanding solar wind have been cited as a possible cause of the decrease [e.g., *Lepping and Behannon*, 1986]. We conclude that this is not possible. In Appendix B, we show that the product $n_{rd}\sigma_{rd}$, where $n_{rd}$ number of RDs per unit volume and $\sigma_{rd}$ is the average area of a RD projected in the radial direction, must decrease with $r$ to account for observations. Purely geometric effects give constant $n_{rd}\sigma_{rd}$.

Thus RDs dissipate entirely or lose part of their area, or RDs undergo some time dependent process which renders them undetectable for increasing amounts of time with increasing $r$. Dissipation is the simpler way to explain a monotonic decrease in RD numbers.

We also show that refraction alone in a medium where the Alfvén speed varies across field lines would actually give increasing $n_{rd}\sigma_{rd}$ after some intermediate travel time from the Sun. Resonant transfer is a candiate to explain the decrease since it can dissipate some RDs. However, since it does not dissipate all of them, we find that it has some disadvantages in explaining the continual and monotonic decrease of RD numbers with increasing $r$. Another possibility is that waves and imbedded RDs propagate through a nearly random medium where $c_A$ varies in all directions. This random medium may also be due to turbulent wave interactions. Travel through this medium might continually "attentuate" coherent structures, such as RDs.

Details of RD evolution can be found in Appendix B.

### 4.4. Proton Heating

Simulations show that resonant transfer among large-amplitude waves containing imbedded RDs can heat protons across large regions and not just on resonant field lines. RDs disrupted by resonant transfer become sources of large-$k$ fluctuations which can pitch angle scatter protons and heat them. This process is also accompanied by a cascade due to wave steepening which provides more energy to the large-$k$ fluctuations than can be provided by the spontaneous dispersion of the RDs at any one time. It is this cascade and the large value of $T_{rt}$ in the solar wind which can sustain the heating for a long period which makes this process of interest.

In section 4.4.1, we briefly discuss the estimated amount of proton heating which could occur between 0.3 and 1 AU if resonant transfer is operating relatively efficiently. Section 4.4.2 examines how waves and particles are likely to interact when a cascade operates so as to produce obliquely propagating waves. We obtain an important inferrence about the nature of wave and particle interactions in the solar wind. Section 4.4.3 discusses how RDs produced in the solar chromosphere could deliver ion cyclotron waves to the corona which could then provide ion heating.

**4.4.1. Solar wind proton heating rate.** In the solar wind, protons show perpendicular heating which increases the magnetic moment by a factor of 2 to 3 between 0.3 and 1 AU [e.g., *Marsch et al.*, 1983]. Heating continues at larger distances [e.g., *Matthaeus et al.*, 1999a]. At 0.3 AU, core temperatures are particularly anisotropic [e.g., *Marsch et al.*, 1982]. This is often attributed to cyclotron resonant heating.

Resonant transfer results in dissipation of wave energy and proton heating. In Appendix C, we estimate the rate of heating from resonant transfer between 0.3 and 1 AU. We assume that there are purely outgoing Alfvén waves in a spherically expanding solar wind and employ a WKB analysis for wave intensities alone. We find that the magnetic moment could be increased by 10% by 1 AU. This is a significant increase but far smaller than the observed 100-200% increases. This shows that other sources of heating predominate.

**4.4.2. Wave-particle interactions.** The cascade and dissipation of wave energy seen in simulations does fit some observed properties of the high-frequency portion of the power spectrum of Alfvénic fluctuations where dissipation is expected to occur. It does not match the observed spectral index because steepening governs this cascade.

*Leamon et al.* [1998a, 1998b; 1999] have used Wind magnetic field data in the high-frequency range and concluded that waves propagate more oblique than parallel. This matches our simulation results because resonant transfer requires oblique wave interactions. Our simulations show that oblique waves at large-$k$ result in second-order Fermi acceleration because particles can then interact with several waves at once. Protons can also interact with the associated compressions of the oblique wave through Landau and transit time damping. We expect these interactions to occur regardless of the exact nature of the cascade whenever oblique waves predominate in the dissipation range. These interactions and the resultant heating differ substantially from the direct cyclotron acceleration of protons due to parallel propagating waves.

*Heinemann* [1999] proposed that solar wind ions are heated by first-order Fermi acceleration, which is the reflection of ions from sources moving in opposite directions, near steepened Alfvénic wavefronts with thicknesses nearly equal to the proton gyroradius. In the simulations this process is not of importance because RDs do not attain such small scales nor do we have Alfvén waves traveling in opposite directions to give multiple reflections.

In addition to protons, alpha particles are an important secondary constituent of the solar wind plasma. These could also be heated in association with waves and imbedded RDs and differently from protons depending on how fast they stream along $\mathbf{B}_0$. We are currently studying their behavior and will not pursue this here.

**4.4.3. Heating in the corona and chromosphere.** The dissipation of imbedded RDs and waves from resonant transfer is strongly dependent on the presence of large-amplitude waves. This would make this process irrelevant to the heating which occurs in the corona near the Sun because wave amplitudes are small and RDs should not be generated. However, there is another possible role for the RD in the coronal heating which we outline below.

The chromosphere is a place where Alfvén waves could generate imbedded RDs. In the chromosphere, Alfvén waves can attain large wave amplitudes ($\sim B_0$) [e.g., *Hollweg*, 1978, 1982b]. *Hollweg* [1982b] has consid-

ered the propagation of linearly polarized Alfvén waves along a vertical $\mathbf{B}_0$ and in a vertically stratified chromosphere. These waves steepen into shocks and heat the medium. Because of the wave polarization and propagation parallel to $\mathbf{B}_0$, RDs did not develop when the waves steepened, and so dissipation of much of the wave into heat was found.

In oblique directions, imbedded RDs would be expected to develop. Heating of ions would become difficult beyond an initial steepening period if these RDs become stable against dispersion and do not dissipate due to background variations in the chromosphere.

Some RDs may reach the corona intact. Under coronal conditions the wave amplitude normalized to $B_0$ is very small. The ineffectiveness of wave steepening for such small-amplitude waves might cause the RDs to disperse and breakup at some point in the corona, perhaps near its base. Some of these waves would be ion cyclotron waves which would propagate until they resonantly heat ions and dissipate.

The significant presence of ion cyclotron waves and kinetic processes in the corona is inferred from recent observations by the Solar and Heliospheric Observatory (SOHO). In the corona, ions are often observed to be much hotter than electrons and the heavy ions, and possibly the protons, have larger perpendicular than parallel temperatures [e.g., *Kohl et al.*, 1998; *Dodero et al.*, 1998]. (An alternative proposal involving shock heating has been offerred by *Lee and Wu* [2000].)

RDs might be a source of ion cyclotron waves in the corona whose importance is not yet determined. Currently, the majority of ion cyclotron waves in the corona are expected to come from local turbulent cascades [e.g., *Hollweg*, 1986, 2000b; *Cramner*, 1999], and from reconnection sites near the coronal base [e.g., *Tu and Marsch*, 1997; *Ruzmaikin and Berger*, 1998]

Since the RDs are likely to have oblique normals, the dispersive spreading of RDs would yield ion cyclotron waves which also propagate obliquely. These oblique waves are compressional and would contribute to the density spectrum detected by interplanetary scintillations [e.g., *Hollweg*, 2000a]. Faraday rotation would also occur [e.g., *Spangler and Mancuso*, 2000]. These observations could test whether the ion cyclotron waves which are mainly repsonsible for coronal heating propagate parallel or oblique. This would further support or eliminate sources, such as RDs, which generate mostly oblique waves.

### 4.5. Kinetic Alfvén Waves

Starting from the average wavenumbers of Alfvénic fluctuations, it would take far too long to reach $k_\perp \sim c/\omega_{pi}$ via refraction. Instead, one must rely on interactions to cascade wave power to these large wavenumbers. For instance, if we want to refract to $c/\omega_{pi} \approx 100$ km at 1 AU where $\delta k_\perp = 0.0628$ km$^{-1}$ over $t = 10$ hours, then using $\delta c_A = 1.5$ km/s and assuming that $k_\parallel \approx 2\pi/L$, we find that $L = 2324$ km or about 23 $c/\omega_{pi}$. Only by starting at such small wavelengths could a conversion to a KAW be possible via refraction from generated PBSs.

## 5. Summary and Conclusions

In a compressible plasma an expansion of the MHD equations in wave amplitude shows that first-order Alfvén waves with the same sign of $k_\parallel$ can generate second-order PBSs in the perpendicular direction. This introduces variations in the Alfvén speed which can lead at higher orders to wave refraction where $k_\parallel$ remains constant and $k_\perp$ increases for long enough times. When the first-order wave also has a magnetic fluctuation component along the direction in which the PBS varies, a resonant transfer of energy across field lines can occur. This transfer is always possible when $\mathbf{B}_0$ lies outside the plane of interaction between wave vectors and is inherently a process which involves oblique waves. It can produce KAWs near resonant field lines.

As a result of the generated PBSs, no exact equilibrium is generally possible even when all the Alfvén waves have the same sign of $k_\parallel$. (An equilibrium would exist in an incompressible plasma because the second-order PBS has zero amplitude and balance is maintained by a mechanical pressure.) The background fields and plasma will generally vary on the scales of the Alfvén waves.

Simulation results of large-amplitude Alfvén wave evolution shows that they tend to steepen and generate imbedded RDs. They also generate PBSs, and so refraction and resonant transfer occur. However, unlike small-amplitude waves, KAWs do not form and wide spread dissipation of wave energy occurs.

Through resonant transfer and refraction, some imbedded RDs can be significantly dissipated and effectively removed in regions where wave energy is mostly transported away. RDs on field lines where little transfer occurs remain intact. As these RDs refract, they are disrupted and emit dispersive and compressional fluctuations which propagate obliquely. This dispersion counteracts the tendency of refracting RDs to approach very small widths.

Protons are heated by these processes through pitch angle scattering from large-$k$ waves moving in different directions. This is second-order Fermi acceleration. Additional heating comes from Landau and transit time damping of the wave compressional component. Sustained heating of protons occurs because resonant transfer initiates a cascade governed by wave steepening which drives energy into the large-$k_\parallel$ and -$k_\perp$ fluctuations which then scatter the protons.

Resonant transfer is a candidate for explaining why RDs occur less frequently with increasing distance in the solar wind. Essentially, it would significantly dissipate those waves and imbedded RDs subjected to energy transport across field lines. This process dissipates only some RDs. Thus it has the disadvantage that it

may not be able to to account for the observed monotonic decrease in RD numbers with increasing distance from the Sun wherein all RDs must eventually be dissipated. This disadvantage might be overcome if waves and RDs propagate in a random medium.

We have estimated the amount of proton heating which might occur in association with resonant transfer due to generated PBSs. We find that it might account for a marginally significant amount (5–10%) of the observed heating between 0.3 and 1 AU.

The manner in which the protons are heated in the simulations could occur in the solar wind. *Leamon et al.* [1998a] find that waves are more obliquely propagating than parallel in the range of wavenumbers where dissipation is expected. Since oblique waves can travel in different directions, we can surmise that heating from second-order Fermi acceleration must occur regardless of how the energy reached the dissipation range. These waves also have associated compressions which can heat protons through Landau and transit time damping.

There is a possible role for RDs in coronal heating. Imbedded RDs could be generated in the chromosphere, where Alfvén waves can have large amplitudes and propagate into the corona. In the corona, wave amplitudes are small, and the nonlinear processes seen in simulations would not occur. Instead, the RDs might simply disperse because nonlinear steepening is unable to maintain balance. This could provide a source of ion cyclotron waves which could then contribute heat to the corona.

## Appendix A: Small-Amplitude Expansions and Solutions

The MHD equations are expanded to order $\eta$. The magnetic field $\mathbf{B}_\eta$, bulk velocity $\mathbf{V}_\eta$, and density $\rho_\eta$ as functions of time $t$ and position are given by

$$\frac{\partial \rho_\eta}{\partial t} = -\sum_{l=0}^{\eta}[\rho_l \nabla \cdot \mathbf{V}_{\eta-l}] \quad \text{(A1)}$$

$$\sum_{l=0}^{\eta}[+(\mathbf{V}_l \cdot \nabla)\rho_{\eta-l}],$$

$$\sum_{l=0}^{\eta} \rho_l \frac{\partial \mathbf{V}_{\eta-l}}{\partial t} = -c_s^2 \nabla \rho_\eta - \sum_{l=0}^{\eta} \nabla \frac{\mathbf{B}_l \cdot \mathbf{B}_{\eta-l}}{8\pi} \quad \text{(A2)}$$

$$+\sum_{l=0}^{\eta}(\mathbf{B}_l \cdot \nabla)\frac{\mathbf{B}_{\eta-l}}{4\pi}$$

$$-\sum_{m=0}^{\eta}\sum_{l=0}^{\eta-m} \rho_m (\mathbf{V}_l \cdot \nabla)\mathbf{V}_{\eta-l-m},$$

$$\frac{\partial \mathbf{B}_\eta}{\partial t} = \sum_{l}^{\eta} \nabla \times (\mathbf{V}_l \times \mathbf{B}_{\eta-l}). \quad \text{(A3)}$$

where these are the continuity, momentum, and induction equations, respectively. We have adopted a polytropic equation of state for the pressure $P$, where $\partial P/\partial x = c_s^2 \partial \rho/\partial x$, $c_s = (\gamma P_0/\rho_0)^{1/2}$ is the sound speed, and $\gamma$ is the specific heat ratio. The background magnetic field $\mathbf{B}_0$ and $\rho_0$ are space constants and $\mathbf{V}_0 = 0$. The first-order solutions are a set of Alfvén waves with the same sign of $k_\parallel$.

To show that the driven solutions give constant $B$ in oblique but not perpendicular directions, we work by induction. First, $\rho_1 = \rho_2 = 0$. The generalized Reynolds stress at third order is then $(\mathbf{B}_1 \cdot \nabla)\mathbf{B}_2/4\pi - \rho_0(\mathbf{V}_1 \cdot \nabla)\mathbf{V}_2 + (\mathbf{B}_2 \cdot \nabla)\mathbf{B}_1/4\pi - \rho_0(\mathbf{V}_2 \cdot \nabla)\mathbf{V}_1$. These magnetic and velocity stresses cancel, and the only remaining driver comes from $-\nabla B^2/8\pi$. Partial differential equations at third order can be derived which couple $\rho_3$ and $B_{3\parallel}$ for each Fourier component of the driver $\mathrm{D}_3 = 2\mathbf{B}_1 \cdot \mathbf{B}_2$. As for (23) and (24) in the work of *Vasquez and Hollweg* [1999], we can write these equations in $k$ space as

$$\frac{\partial^2 \rho_3}{\partial t^2} + c_s^2 k^2 \rho_3 = -\frac{k^2 \mathrm{D}_{3k}}{8\pi} - \frac{B_0 k^2 B_{3\parallel}}{4\pi} \quad \text{(A4)}$$

$$\frac{\partial^2 B_{3\parallel}}{\partial t^2} + c_A^2 k^2 B_{3\parallel} = -\frac{B_0 k_\perp^2 c_s^2 \rho_3}{\rho_0} - \frac{B_0 k_\perp^2 \mathrm{D}_{3k}}{8\pi\rho_0}, \quad \text{(A5)}$$

where $\mathrm{D}_{3k} = (\mathrm{D}_3 - \langle \mathrm{D}_3 \rangle)_k$ is the Fourier component of the driver. (Note that $c_s^2$ and $c_A^2$ are the background values of the sound speed and Alfvén speed, respectively.) Since these equations have an equivalent form with the second-order ones, we know that the driven solution will give $B$ constant to third order and $\rho_3 = 0$. Repeating this process at fourth order, we get equations of similar form. By induction, $\rho_\eta = 0$ for $\eta \geq 1$, and $B_{\eta\parallel}$ is given by (2).

A simplified solution is obtained if the first-order fluctuations are polarized along a single axis. Then, $\mathbf{B}_1$ is orthogonal to $\mathbf{B}_2$, so that the driven term at third order due to $\mathbf{B}_1 \cdot \mathbf{B}_2$ vanishes, and so there are no driven fluctuations at third order (i.e., $\mathbf{B}_3 = 0$). At successively higher orders, we find $\mathbf{B}_1$ is always orthogonal to higher-order magnetic fluctuations. This combined with the vanishing of odd lower-order fluctuations leads by induction to the conclusion that only even powers of $\mathbf{B}_\eta$ for $\eta \geq 2$ are nonzero.

When there is a single Alfvén wave at first order, our solutions predict a constant-$B$ wave at all orders. *Barnes and Hollweg* [1974] found an exact constant-$B$ solution for the case of a single first-order Alfvén wave with a sinusoidal waveform. We let the first-order Alfvén wave be polarized in the $z$ direction, and let $B_z = A\cos\phi$, where $\phi = k_x x + k_y y - c_A|k_x|t$. The driven magnetic field $\mathbf{B}_p$ lies in the $xy$ plane with $\mathbf{B}_0 = B_{0x}\hat{\mathbf{x}}$ and is perpendicular to $\mathbf{k}$ so that $\mathbf{B}_p = B_x\hat{\mathbf{x}} - k_x B_x/k_y\hat{\mathbf{y}}$. The magnitude of $\mathbf{B}_p$ can be written as

$$B_p = \sqrt{C^2 - A^2\cos^2\phi} - B_{0p}, \quad \text{(A6)}$$

where $B_{0p} = \mathbf{B}_0 \cdot \mathbf{B}_p/B_p$ and $C$ is a constant magnetic intensity. Since we always solve for the par-

allel component $B_x$, we can relate this to $B_p$ using $B_p = (1+k_x^2/k_y^2)^{-1/2}B_x$. If (A6) is expanded in powers of $A$, it is clearly an even power series, as is expected. The value of $C$ is unspecified, and Barnes and Hollweg determined its value by root finding and numerical integration. *Vasquez and Hollweg* [1996a] expressed $C$ in terms of an elliptical integral. A power series for $C^2$ can be written using $< \mathrm{D}_\eta >$ and gives

$$C^2 = B_{0p}^2 + \frac{A^2}{2} + \frac{A^4}{32B_{0p}^2} + \cdots. \quad \text{(A7)}$$

Convergence is rapid for $A/B_{0p} \ll 1$, and good accuracy is achieved with only a few terms.

In the perpendicular direction, wave-wave or PBS-PBS interactions continue to give driven structures which satisfy pressure balance at higher orders.

At third order in (A1)-(A3) the interaction of a first-order Alfvén wave and a second-order PBS which has finite $B_{2x}(y,z)$ and $\rho_2(y,z)$ would give

$$\frac{\partial \rho_3}{\partial t} = -\rho_0 \nabla \cdot \mathbf{V}_3 - (\mathbf{V}_1 \cdot \nabla)\rho_2, \quad \text{(A8)}$$

$$\rho_0 \frac{\partial \mathbf{V}_3}{\partial t} + \rho_2 \frac{\partial \mathbf{V}_1}{\partial t} = -c_s^2 \nabla \rho_3 - \frac{1}{4\pi}\nabla(\mathbf{B}_0 \cdot \mathbf{B}_3) + (\mathbf{B}_0 \cdot \nabla)\frac{\mathbf{B}_3}{4\pi} + (\mathbf{B}_1 \cdot \nabla)\frac{\mathbf{B}_2}{4\pi} + (\mathbf{B}_2 \cdot \nabla)\frac{\mathbf{B}_1}{4\pi} \quad \text{(A9)}$$

$$\frac{\partial \mathbf{B}_3}{\partial t} = \nabla \times (\mathbf{V}_1 \times \mathbf{B}_2 + \mathbf{V}_3 \times \mathbf{B}_0). \quad \text{(A10)}$$

First, we consider the case where the PBS varies only in the $y$ direction and $\mathbf{B}_0$ lies along the $x$ axis. If the Alfvén wave is polarized along the $z$ axis, then we can derive (3)-(4). The equations are secular and can be solved as given in section 2.2. The solution shows that the Alfvén wave undergoes only refraction.

The general case has the PBS varying both in $y$ and $z$, and/or an Alfvén wave with at least one fluctuation component in a direction of variation. One can take the Fourier transform in space of (A8)-(A10) and then the Laplace transform in time. Secularity can arise only at the Alfvén pole of the Laplace transform (i.e., $s^2+\omega^2$, where $s^2$ is the Laplace transform of $\partial^2/\partial t^2$ for vanishing initial conditions and $\omega^2 = c_A^2 k_\parallel^2$). Secularity is avoided at first by obtaining two coupled equations for $\rho_3$ and $B_{3x} = B_{3\parallel}$, using a procedure outlined by *Vasquez and Hollweg* [1999] for second order. The transformed quantities, denoted by $\hat{\rho}_3$ and $\hat{B}_{3\parallel}$, satisfy

$$s^2\hat{\rho}_3 = -c_s^2 k^2 \hat{\rho}_3 - \frac{B_{0x}}{4\pi}k^2 \hat{B}_{3\parallel} + \frac{\hat{D}}{s^2+\omega^2} \quad \text{(A11)}$$

$$s^2\hat{B}_{3\parallel} = -\frac{B_{0x}}{\rho_0}c_s^2 k_\perp^2 \hat{\rho}_3 - c_A^2 k^2 \hat{B}_{3\parallel}, \quad \text{(A12)}$$

where $\hat{D}/(s^2+\omega^2)$ is the Laplace and Fourier transform of the driver term $(\mathbf{B}_1 \cdot \nabla)B_{2\parallel}/4\pi$. These equations can be solved individually for the different Fourier components of the driver which come from the sum and difference of the wave and PBS wave vectors. The homogeneous solutions belong to magnetosonic modes and so are not secular with the driver. The driven solution has the following form:

$$\hat{\rho}_3 = \frac{-1}{c_A^2 k_\parallel^2}\frac{\hat{D}}{s^2+\omega^2} \quad \text{(A13)}$$

$$\hat{B}_{3\parallel} = \frac{B_{0x}c_s^2}{\rho_0 c_A^4 k_\parallel^2}\frac{\hat{D}}{s^2+\omega^2}. \quad \text{(A14)}$$

The inverse transforms of (A13) and (A14) give a compressive wave which propagates at the speed of an Alfvén wave. The original incompressible Alfvén wave has now acquired a weak compressive component in the nonuniform medium. This third-order wave has the polarization of a magnetosonic wave, and the rest of its field and velocity components can solved using this polarization [*Vasquez and Hollweg*, 1999].

The drivers in (A9) and (A10) for $V_{3y}$, $V_{3z}$, $B_{3y}$, and $B_{3z}$ are not satisfied by the solutions from the magnetosonic part. This leaves homogeneous Alfvén waves and drivers with the same frequency. The secular part of these equations can handled as in section 2.2. Equations can be reduced to two depending separately on $B_{3y}$ and $B_{3z}$ which give refraction. Resonant transfer must also arise in this situation. This can deduced as in section 2.2.2 through the coupling between $B_y$ and $B_z$ imposed by $\nabla \cdot \mathbf{B} = 0$.

As $\eta \to \infty$, we would expect our analysis to lead to an infinite number of Fourier components from the interaction of a wave and a PBS. These are not new Alfvén waves. Instead, they represent deviations from the plane-wave solutions at first order due to refraction and resonant transfer. The additional Fourier components describe the rippling of the wave front and the variation of amplitude along the front. Refraction and resonant transfer are linear wave processes. This motivates finding a more compact presentation of this behavior which does not Fourier transform in the perpendicular directions in which the PBSs vary.

The Laplace transform satisfies causality by means of a step or Heaviside function which is zero for $t < 0$ and unity for $t \geq 0$. This function multiplies all solutions of the transformed equations. As a result, the driven and homogeneous solutions exist even at $t = 0$. Of course, the exact nonlinear solutions would have to generate these over a period of time. However, for small amplitudes the asymptotics is such that a good enough solution can be developed with a sum of driven and homogeneous solutions existing for $t \geq 0$. This shows that we could generate a new expansion of the MHD equations by treating the PBS solutions as if they existed initially and at zeroth order. We could similarly take the exact constant-$B$ wave solutions and promote them

up to zeroth-order and examine how nonuniformity influences evolution. However, this situation has not been examined in previous work. Instead, wave fluctuations are expanded in wave amplitude. The first-order equations have been solved and analyzed.

We can generate a set of first-order equations similar to those analyzed by *Hollweg and Yang* [1988], who examined PBSs varying in one direction only. For our case, we have

$$\frac{\partial \rho_1}{\partial t} = -\rho_0 \nabla \cdot \mathbf{V}_1 + (\mathbf{V}_1 \cdot \nabla)\rho_0, \quad \text{(A15)}$$

$$\rho_0 \frac{\partial \mathbf{V}_1}{\partial t} = -c_s^2 \nabla \rho_1 - \nabla \frac{B_{0x} B_{1x}}{8\pi} + \frac{B_{0x}}{4\pi} \frac{\partial \mathbf{B}_1}{\partial x} + (\mathbf{B_1} \cdot \nabla) \frac{\mathbf{B_0}}{4\pi} \quad \text{(A16)}$$

$$\frac{\partial \mathbf{B}_1}{\partial t} = \nabla \times (\mathbf{V}_1 \times \mathbf{B}_0). \quad \text{(A17)}$$

Equations (A15)-(A17) are linear but have nonconstant coefficients due to variations of $\rho_0$ and $B_{0x}\hat{\mathbf{x}}$ in the $y$ direction. These equations possess solutions of the form $e^{i(k_x x + k_z z - \omega t)}$ which can be used to transform the equations to a set of ordinary differential equations in $y$. These will be equivalent to (8), (9), and (15) of *Hollweg and Yang* [1988], except that they use $k_z = 0$ and $B_{0z} \neq 0$. Following the analysis of *Hollweg and Yang* [1988], the ordinary differential equations can be shown to have singular points on resonant field lines. These are true resonances. With increasing time the wave amplitude will become infinite on these lines. Physics outside of ideal MHD must be considered to understand the ultimate outcome of wave evolution along resonant field lines.

The sonic Mach number expansions of *Bhattacharjee et al.* [1998, 1999] study the role of nonuniformities on nonlinear Alfvén waves. However, they start with two assumptions which are not justified dynamically. First, they include nonuniformities at zeroth order as an initial condition which can be prescribed without reference to waves. Second, they assume that $k_{\|} \ll k_{\perp}$ for all fluctuations. Our analysis gives a dynamic justification for these assumptions. First, we have shown that nonlinear Alfvén waves in an initially uniform medium will generate a nonuniform one. Second, wave vectors evolve such that $k_{\|}$ remains constant but $k_{\perp}$ increases without limit at long times (i.e., $t > T_{ca}$).

## Appendix B: RD Normals and Occurrence Rates

In this appendix, we examine the theoretical principles which underlie the behavior of RD normals and occurrence frequency in nonuniform solar wind. These results should prove useful in further statistical studies of solar wind RDs and in theoretical studies.

### B.1. RD Normals

For waves and imbedded RDs in a radially expanding solar wind, the wave vectors and normals should tend to the radial direction. The observed distribution of RD normals near 1 AU shows that they are scattered in nearly all directions around $\mathbf{B}_0$ [e.g., *Smith*, 1973]. This indicates refraction due to gradients of the Alfvén speed across the magnetic field lines. Generated PBSs can contribute to this effect.

Nearly field-aligned RD normals are as numerous as ones in other directions. The lack of a strong clustering of normals in the perpendicular direction suggests that not many $T_r$ periods have occurred since their formation, which is consistent with the value of $T_r$ calculated in section 4.1. Thus, near 1 AU, we have an intermediate situation, depicted in Figure 1, where some initially oblique normals can become more field aligned. This intermediate situation can be prolonged if the wave speed gradients are more random in distribution and not limited to the perpendicular direction.

### B.2. Geometric Effects on RD Occurrence Rates

If RDs are isolated phase surfaces, one might expect that the expanding solar wind would drive them further apart. A single spacecraft may then have a lower probability of detecting RDs with increasing $r$. We call this the fragmentation hypothesis.

We assume that there are RDs imbedded in an Alfvén wave separated from one another by one half of the wavelength of the Alfvén wave. They have continuous phase surfaces at some distance near the Sun and span a number of field lines. In a uniform solar wind their surfaces would remain intact and always span the same number of field lines. Without gaps in the phase surfaces we would expect that these RDs to have the highest probability of detection by a single spacecraft at all $r$.

Now consider that these RDs span a number of flux tubes bounded by TDs. Each flux tube is uniform within but can differ from another tube. These RD phase surfaces can be reduced to a number of isolated fragments because the speed of convection $V_{sw}$ by the solar wind and/or speed of propagation $c_A$ can vary between adjacent flux tubes or the flux tubes may have different path lengths if they are not parallel to one another. Once some space opens between the fragments, a single spacecraft would have less chance of detecting RDs.

This approach seems to justify the hypothesis that geometric effects of solar wind expansion lead to lower probabilities of detection. However, the hypothesis is flawed. If one actually followed the progress of these fragments, one could show that the probability of detection actually fluctuates with increasing $r$ and does not decrease monotonically so as to match observed RD behavior. In fact, it is possible that the fragments from different initial phase surfaces could be combined into

a phase surface at some $r$ which has the same area as one of the original RDs.

In order to do this correctly, one cannot start with continuous phase surfaces. One should assume that the RDs are a set of isolated fragments at the starting distance. Over a statistical ensemble we would expect that as many RDs along the TD boundaries are approaching one another as are receding. We can then determine the occurrence frequency $\nu_{rd}$ as

$$\nu_{rd} = n_{rd}\sigma_{rd}(V_{sw} + c_A \mathbf{B}_0 \cdot \hat{\mathbf{r}}). \quad \text{(B1)}$$

In (B1), $n_{rd}$ is the number of RDs per unit volume, $\sigma_{rd}$ is the typical area of a RD projected into the radial direction, and the terms in parenthesis are the mean radial speed that the RDs pass the spacecraft assuming that all RDs travel away from the Sun. This frequency is calculated in the same manner as the collision frequency of particles.

With increasing $r$ the mean radial speed can decrease because $c_A$ decreases. However, $c_A \ll V_{sw}$ for $r > 0.3$ AU, and this effect is small compared to the observed decrease of $\nu_{rd}$. Thus significant changes in $\nu_{rd}$ must come from the product $n_{rd}\sigma_{rd}$.

If we assume that RDs remain intact at all times, then $n_{rd}$ varies only with respect to a unit volume. In the solar wind, expansion causes the occupied volume of RDs to increase as $r^2$. Hence $n_{rd} \propto r^{-2}$. Assuming that the RD normals are isotropically distributed, as is observed, $\sigma_{rd} \propto r^2$. This occurs because Alfvén waves and imbedded RDs always span the same number of field lines at all $r$ within a uniform flux tube. The cross-sectional area of a tube in the radial direction expands as $r^2$, and so it follows that RDs will behave similarly. Thus $n_{rd}\sigma_{rd}$ does not vary with $r$.

In the solar wind we cannot simply assume that we are losing RDs imbedded in Alfvén waves, as if they were leaves scattered in a breeze. The actual geometric effect of the expanding solar wind is to keep $\nu_{rd}$ nearly constant with $r$.

### B.3. Imbedded RDs Evolving By Refraction Alone

Figure 1 shows the refraction of a phase front. With increasing time, one can infer from Figure 1 that the total length (say $|\ell|$) of the phase lines grows with time everywhere when $t > T_{ca}$. The length is a constant only in a direction along $\mathbf{B}_0$ (i.e., $|\ell \cdot \mathbf{B}_0|$).

We can relate the length of the phase lines in Figure 1 to the area $\sigma_{rd}$. After sufficient time ($t > T_{ca}$), RD normals begin refracting to more oblique directions, and $\sigma_{rd}$ would increase in directions other than along $\mathbf{B}_0$. In the solar wind, observations are made in the radial direction which differs from the direction of $\mathbf{B}_0$ at most distances from the Sun. An increase of $\sigma_{rd}$ with time and so with distance from the Sun without the removal of some RDs would increase the probability of a detection by a spacecraft. This is contrary to observations.

Refraction causes the width of a RD to decrease as its normal turns oblique, due to increasing $k_\perp$. Far from the Sun, one would expect to observe preferentially thinner RDs with increasing distance, which is not seen. Wave dispersion can be expected to oppose this behavior, and simulation results show that it counteracts this tendency.

### B.4. Evolving by Resonant Transfer and Refraction

Because resonant transfer can dissipate RDs, it is a candidate for explaining the disappearance of RDs in the solar wind. In the simulations, only some RDs can be dissipated strongly. The remaining RDs refract into oblique directions which in the solar wind would imply an increasing occurrence rate. Moreover, simulation results do not rule out forming new RDs.

In order to recover the monotonical decrease $\nu_{rd}$ with increasing $r$, two conditions must be satisfied. First, waves and imbedded RDs which are stable or nearly stable to resonant transfer at some distance $r_1$, must become significantly unstable at some $r_2 > r_1$. Second, the dissipation rate of RDs must be greater than the formation rate.

### B.5. Evolution in a Random Medium

There is a potentially important aspect of RD behavior not contained in our simulations. In the solar wind a random medium could arise through which waves and RDs must propagate. Wave speed variations would exist in all directions and not preferentially in the perperdicular direction. These variations could arise from waves or from preexisting solar ones. Turbulence may also account or contribute to a random medium.

In a random medium we could describe the evolution of RDs from the viewpoint of coherence. Close to the Sun, steepening of Alfvénic fluctuations gives rise to ordered structures, the RDs, which have coherent phase surfaces with transverse dimensions far larger than their widths. With increasing distance the propagation through the random medium causes a loss of coherence, and so RDs, and ultimately dissipation. A decrease in wave coherence with $r$ would also reduce the chances that a new RD would form by wave steepening. We would expect this loss to obey a monotonically decreasing function with distance traveled through the random medium. As such, this gives an attractive but unproven explanation for the observed behavior of $\nu_{rd}$.

## Appendix C: Estimate of Solar Wind Proton Heating

In principle, we can say that the dissipation of any RD should give heating to protons. The important but difficult to answer question is how much heat would be given to protons in the solar wind. This is difficult because the heating arises in a process dependent upon the initial state. Our initial state of two interacting Alfvén waves is certainly too simple for the solar wind. Additionally, the compressions generated by the waves are far larger than what is seen in the solar wind. Thus

we will not use the heating rate determined from simulations to estimate heating in the solar wind.

We will assume at all $r$ that some wave energy is subject to resonant transfer due to preexisting PBSs which vary exactly in the perpendicular direction at all $r$. On the basis of section 4.2 the rate of transfer is taken to vary as

$$T_{rt} = T_{rt0}\frac{r}{r_0}, \tag{C1}$$

where $T_{rt0}$ = 19 hours = 68,400 s at $r_0$ = 0.3 AU. We have derived (C1) using values from section 4.2 and assuming that in (10) $\Delta c_A$ is a space constant between 0.3 and 1 AU and $L$ varies as $r/r_0$. Somewhat less heating is obtained if $T_{rt}$ = 38 hours = 136,800 s is taken to be a space constant.

We denote the sum of magnetic and kinetic wave energy by $W$. One half of the $W$ is transferred in time $T_{rt}$. Assuming that the Alfvén waves and imbedded RDs have a nearly isotropic distribution of wave vectors, then nearly one half of the wave power is associated with a direction in which the Alfvén speed varies across field lines. We further divide this by one half to account for those waves which are not refracting to larger angles with respect to $\mathbf{B}_0$. Thus, at any given $r$, only $W/8$ is involved in a transfer.

We assume that all transferred energy immediately dissipates. The heating rate $\dot{Q}$ is then $(W/8)/T_{rt}$. This heating will be equipartitioned to all three temperature components.

We will use the heating rate to compute the increase of the proton magnetic moment $\mu_{ad}(= v_{th,\perp}^2/2B)$ or first adiabatic invariant between 0.3 and 1 AU. Assuming bi-Maxwellian distributions, the magnetic moment of a proton at the thermal speed $v_{th,\perp} = (2T_\perp)^{1/2}$ normalized to the Alfvén speed will be studied since it relates directly to $T_\perp$. Without heating, $\mu_{ad} = T_\perp/B$ should be constant with $r$, and so it is a sensitive indicator of heating processes in the solar wind. The average observed increase of $\mu_{ad}$ in the solar wind over these distances is by factors of 2 or 3 [e.g., *Marsch et al.*, 1983].

At 0.3 AU the average perpendicular temperature is $10^6 K$, whereas the parallel temperature is one half of this. The magnetic field intensity is near 48 nT and the proton number density is 50 $cm^{-3}$. In dimensionless units, $T_\perp$ = 0.25, which means that the kinetic energy is one half of the background magnetic energy at 0.3 AU, which is $B_0^2/2$ = 0.5. We will assume a radial background magnetic field $B = B_0(r/r_0)^{-2}$ and number density $n = n_0(r/r_0)^{-2}$. At $r_0$ = 0.3 AU we take $B_0 = n_0 = 1$ in our dimensionless units. If no heating occurs, then $T_\perp = 0.25(r/0.3)^{-2}$ with $r$ given in AU. At 1 AU, $T_\perp$ = 0.0225 in terms of the magnetic energy at 0.3 AU. The value of $\mu_{ad}$ would be a constant equal to 0.25.

The addition of heating causes $\mu$ to increase as

$$\frac{d\mu_{ad}}{dr} = \frac{\dot{Q}}{3V_{sw}nB} = \frac{Wr^3}{24V_{sw}T_{rt0}r_0^3}, \tag{C2}$$

where $V_{sw}$ is the velocity of the solar wind in AU per second and only one third of the total heating rate contributes.

The variation of $W$ with $r$ is needed to solve (C2). Assuming wavelengths are small compared to $r$ and since we neglect backward waves, we use a WKB analysis to estimate $W(r)$. For $r \gtrsim 0.3$ AU, we can reasonably take $V_{sw}$ to be a constant and neglect the contribution of the wave propagation speed to the energy flux of Alfvén waves [e.g., *Hollweg*, 1981]. Then, at lowest order, a WKB expansion shows that $W$ can be found from this energy flux equation

$$\frac{dW}{dr} = -\frac{\dot{Q}}{V_{sw}} - \frac{3W}{r}, \tag{C3}$$

where the first term on the right-hand side is from the total amount of wave energy dissipated due to proton heating and the second term is the loss of wave energy from the work they perform on the solar wind [e.g., *Hollweg*, 1981]. Without, dissipation $W = W_0(r/r_0)^{-3}$.

At $r_0$ = 0.3 AU we assume that the Alfvén waves have relative amplitudes of 0.5. Thus we take $W_0$ = 0.25. We take $V_{sw}$ = 500 km/s = $3.33 \times 10^{-6}$ AU/s.

First, we solve for $W$ from (C3) and find that $W = W_0(r/r_0)^{-(3+\chi)}$, where $\chi = r_0/(8V_{sw}T_{rt0})$. For the chosen parameters, $\chi$ = 0.165, and 18% of the energy dissipates relative to $r^{-3}$ rate at 1 AU. Substituting the solution for $W$ into (C2) and integrating, we find

$$\mu_{ad} - \mu_{ad0} = \frac{W_0 r_0^\chi}{24V_{sw}T_{rt0}}\frac{r^{1-\chi} - r_0^{1-\chi}}{1-\chi} \tag{C4}$$

With $\mu_{ad0}$ = 0.25 this gives $\mu$ = 0.292 at $r$ = 1, which is a 17% increase.

The same amount of heat should occur in the parallel direction. Heating of $T_\parallel$ is more complicated to study due to heat fluxes. *Marsch et al.* [1983] report that the second adiabatic invariant is approximately obeyed. In a purely radial magnetic field, $T_\parallel$ should then be constant with $r$ without dissipation. At 0.3 AU, $T_\parallel$ = 0.125 and the amount of heating estimated would change this by 7% at $r$ = 1.

In principle, purely outgoing Alfvén waves could heat protons by a significant amount. We have attempted to make assumptions so that the estimated heating is approximately the maximum expected. Since this heating is far from the 100 to 200% increases of $\mu_{ad}$ which are observed, we conclude that resonant transfer from generated PBSs may only be marginally significant in the solar wind. To increase its importance would require having higher rates of refraction and resonant transfer due to additional sources of nonuniformity in the solar wind, which is possible.

The estimated heating also implicates that a process of a different origin is the dominant heating mechanism in the solar wind and is presumably due to a different type of cascade [e.g., *Tu*, 1988; *Hollweg*, 1986; *Matthaeus et al.*, 1999a].

**Acknowledgments.** This work was supported by the NSF under grant ATM-9622057 and ATM-9902904 and by the NASA Sun-Earth Connection Theory Program under grants NAG5-1479 and NAG5-8228 to the University of New Hampshire. We thank P. Isenberg, M. Lee, and S. Markovskii for helpful discussions.

## References

Barnes, A., and J. V. Hollweg, Large-amplitude hydromagnetic waves, *J. Geophys. Res.*, *79*, 2302, 1974.

Bavassano, B., M. Dobrowolny, F. Mariani, and N. F. Ness, Radial evolution of power spectra of interplanetary Alfvénic turbulence, *J. Geophys. Res.*, *87*, 3617, 1982.

Behannon, K. W., Heliocentric distance dependence of the interplanetary magnetic field, *Rev. Geophys. and Sp. Phys.*, *16*, 125, 1978.

Belcher, J. W., and L. Davis, Large-amplitude Alfvén waves in the interplanetary medium, 2, *J. Geophys. Res.*, *76*, 3534, 1971.

Bhattacharjee, A., C. S. Ng, and S. R. Spangler, Weakly compressible magnetohydrodynamic turbulence in the solar wind and the interstellar medium, *Astrophys. J.*, *494*, 409, 1998.

Bhattacharjee, A., C. S. Ng, S. Ghosh, and M. L. Goldstein, A comparative study of four-field and fully compressible magnetohydrodynamic turbulence in the solar wind, *J. Geophys. Res.*, *104*, 24,835, 1999.

Cohen, R. H., and R. M. Kulsrud, Nonlinear evolution of parallel-propagating hydromagnetic waves, *Phys. Fluids*, *17*, 2215, 1974.

Coleman, P. J., Turbulence, viscosity, and dissipation in the solar-wind plasma, *Astrophys. J.*, *153*, 371, 1968.

Cranmer, S. R., G. B. Field, and J. L. Kohl, The impact of ion-cyclotron wave dissipation on heating and accelerating the fast solar wind, in *Solar Wind Nine*, edited by S. R. Habbal, R. Esser, J. V. Hollweg, and P. A. Isenberg, p. 35, Am. Inst. of Phys., College Park, Md., 1999.

Dodero, M. A., E. Antonucci, et al., Solar wind velocity and anisotropic coronal kinetic temperature measured with the O VI doublet ratio, *Sol. Phys.*, *183*, 77, 1998.

Gekelman, W., S. Vincena, D. Leneman, and J. Maggs, Laboratory experiments on shear Alfvén waves and their relationship to space plasmas, *J. Geophys. Res.*, *102*, 7225, 1997.

Ghosh, S., W. H. Matthaeus, D. A. Roberts, and M. L. Goldstein, The evolution of slab fluctuations in the presence of pressure-balanced magnetic structures and velocity shears, *J. Geophys. Res.*, *103*, 23,691, 1998.

Goldstein, B. E., M. Neugebauer, and E. J. Smith, Alfvén waves, alpha particles, and pickup ions in the solar wind, *Geophys. Res. Lett.*, 22, 3389, 1995.

Goldstein, M. L., D. A. Roberts, A. E. Deane, S. Ghosh, and H. K. Wong, Numerical simulation of Alfvénic turbulence in the solar wind, *J. Geophys. Res.*, *104*, 14,437, 1999.

Goossens, M., M. S. Ruderman, and J. V. Hollweg, Dissipative MHD solutions for resonant Alfvén waves in 1-dimensional magnetic flux tubes, *Solar Phys.*, *157*, 75, 1995.

Hasegawa, A., and C. Uberoi, The Alfvén Wave, *Rep. DOE/TIC 11197*, Tech. Inform. Cent., U.S. Dep. of Energy, Washington, D. C., 1982.

Hau, L.-N., and B. U. Ö. Sonnerup, Self-consistent gyroviscous fluid model of rotational discontinuities, *J. Geophys. Res.*, *96*, 15,767, 1991.

Heinemann, M., Normals of non-WKB Alfvén waves in the solar wind, *J. Geophys. Res.*, *85*, 3435, 1980.

Heinemann, M., Solar wind heating by Fermi acceleration, in *Solar Wind Nine*, edited by S. R. Habbal et al., *AIP Conf. Proc.*, *471*, 453, 1999.

Hollweg, J. V., Alfvén wave refraction in high-speed solar wind streams, *J. Geophys. Res.*, *80*, 908, 1975.

Hollweg, J. V., Alfvén waves in the solar atmosphere, *Sol. Phys.*, *56*, 305, 1978.

Hollweg, J. V., Alfvén waves in the solar atmosphere, 2, Open and closed magnetic flux tubes, *Sol. Phys.*, *70*, 25, 1981.

Hollweg, J. V., Surface waves on solar wind tangential discontinuities, *J. Geophys. Res.*, *87*, 8065, 1982a.

Hollweg, J. V., Alfvén waves in the solar atmosphere, 3, Nonlinear waves on open flux tubes, *Sol. Phys.*, *75*, 35, 1982b.

Hollweg, J. V., Transition region, corona, and solar wind in coronal holes, *J. Geophys. Res.*, *91*, 4111, 1986.

Hollweg, J. V., The kinetic Alfvén wave revisited, *J. Geophys. Res.*, *104*, 14,811, 1999.

Hollweg, J. V., Compressibility of ion cyclotron and whistler waves: Can radio measurements detect high-frequency waves of solar origin in the corona?, *J. Geophys. Res.*, *105*, 7573, 2000a.

Hollweg, J. V., Cyclotron resonance in coronal holes, 3, A five-beam turbulence-driven model, *J. Geophys. Res.*, *105*, 15,699, 2000b.

Hollweg, J. V., and G. Yang, Resonance absorption of compressible magnetohydrodynamic waves at thin "surfaces," *J. Geophys. Res.*, *93*, 5423, 1988.

Inhester, B., A drift-kinetic treatment of the parametric decay of large-amplitude waves, *J. Geophys. Res.*, *95*, 10,525, 1990.

Kaghashvili, E. K., On the acceleration of the solar wind: Role of the inhomogeneous flow, *Astrophys. J.*, *512*, 969, 1999.

Karimabadi, H., D. Krauss-Varban, and T. Terasawa, Physics of pitch-angle scattering and velocity diffusion, 1, Theory, *J. Geophys. Res.*, *97*, 13,853, 1992.

Kohl, J. L., et al., UVCS/SOHO empirical determination of anisotropic velocity distributions in the solar corona, *Astrophys. J.*, *501*, L127, 1998.

Leamon, R. J., C. W. Smith, N. F. Ness, and W. H. Matthaeus, Observational constraints on the dynamics of the interplanetary magnetic field dissipation range, *J. Geophys. Res.*, *103*, 4775, 1998a.

Leamon, R. J., W. H. Matthaeus, C. W. Smith, and H. K. Wong, Contribution of cyclotron-resonant damping to kinetic dissipation of interplanetary turbulence, *Astrophys. J. Lett.*, *507*, 181, 1998b.

Leamon, R. J., C. W. Smith, N. F. Ness, and H. K. Wong, Dissipation range dynamics: Kinetic Alfvén waves and the importance of $\beta_e$, *J. Geophys. Res.*, *104*, 22,331, 1999.

Lee, L. C., and B. H. Wu, Heating and acceleration of protons and minor ions by fast shocks in the solar corona, *Ap. J.*, *535*, 1014, 2000.

Lee, M. L., and B. Roberts, On the behavior of hydromagnetic surface waves, *Astrophys. J.*, *240*, 693, 1986.

Lepping, R. P., and K. W. Behannon, Magnetic field directional discontinuities: Characteristics between 0.46 and 1.0AU, *J. Geophys. Res.*, *91*, 8725, 1986.

Lysak, R. L., and W. Lotko, On the kinetic dispersion relation for shear Alfvén waves, *J. Geophys. Res.*, *101*, 5085, 1996.

Machida, S., S. R. Spangler, and C. K. Goertz, Simulation of amplitude-modulated circularly polarized Alfvén waves for beta less than one, *J. Geophys. Res.*, *92*, 7413, 1987.

Malara, F., P. Veltri, and P. Petkaki, Fast dissipation of Alfvén waves in 3D force-free magnetic structres, in *Solar Wind Nine*, edited by S. R. Habbal et al., *AIP Conf. Proc.*, *471*, 353, 1999.

Mariani, F., B. Bavassano, and U. Villante, A statistical study of MHD discontinuities in the inner solar system: Helios 1 and 2, *Sol. Phys.*, *83*, 349, 1983.

Marsch, E., K.-H. Mühlhäuser, R. Schwenn, H. Rosenbauer, W. Philipp, and F. M. Neubauer, Solar wind protons: Three-dimensional velocity distributions and derived plasma parameters measured between 0.3 and 1 AU, *J. Geophys. Res.*, *87*, 52, 1982.

Marsch, E., K.-H. Mühlhäuser, H. Rosenbauer, and R. Schwenn, On the equation of state of solar-wind ions derived from Helios measurements, *J. Geophys. Res.*, *88*, 2982, 1983.

Matthaeus, W. H., and M. L. Goldstein, Measurement of the rugged invariants of magnetohydrodynamic turbulence in the solar wind, *J. Geophys. Res.*, *87*, 6011, 1982.

Matthaeus, W. H., S. Ghosh, S. Oughton, and D. A. Roberts, Anisotropic three-dimensional MHD turbulence, *J. Geophys. Res.*, *101*, 7619, 1996.

Matthaeus, W. H., G. P. Zank, C. W. Smith, and S. Oughton, Turbulence, spatial transport, and heating of the solar wind, *Phys. Rev. Lett.*, *82*, 3444, 1999a.

Matthaeus, W. H., G. P. Zank, S. Oughton, D. J. Mullan, and P. Dmitruk, Coronal heating by magnetohydromagnetic turbulence driven by reflected low-frequency waves, *Astrophys. J.*, *523*, L93, 1999b.

Medvedev, M. V., V. I. Shevchenko, P. H. Diamond, and V. L. Galinsky, Fluid models for kinetic effects on coherent nonlinear Alfvén waves, II, Numerical solutions, *Phys. Plasmas*, *4*, 1257, 1997.

Murawski, K., C. R. DeVore, S. Parhi, and M. Goossens, Numerical simulation study of MHD wave excitation in bounded plasma slabs, *Planet. Space Sci.*, *44*, 253, 1996.

Neubauer, F. M., Nonlinear interaction of discontinuities in the solar wind and the origin of slow shocks, *J. Geophys. Res.*, *81*, 2248, 1976.

Neubauer, F. M., and H. Barnstorf, Recent observational and theoretical results on discontinuities in the solar wind, in *Solar Wind Four*, edited by H. Rosenbauer, *Rep. MPAE-W-100-81-31*, pp. 168-178, Max-Planck-Inst. für Aeron., Katlenburg-Lindau, Germany, 1981.

Neugebauer, M., The structure of rotational discontinuities, *Geophys. Res. Lett.*, *16*, 1261, 1989.

Neugebauer, M., Knowledge of coronal heating and solar-wind acceleration obtained from observations of solar wind near 1AU, in *Solar Wind Seven, 3rd Cospar Conference Proceeding*, edited by E. Marsch and R. Schwenn, p. 69, Pergamon, New York, 1992.

Ofman, L., and J. M. Davila, Solar wind acceleration by solitary waves in coronal holes, *Astrophys. J.*, *476*, 357, 1997.

Oughton, S., E. R. Priest, and W. H. Matthaeus, The influence of a mean magnetic field on three-dimensional magnetohydrodynamic turbulence, *J. Fluid Mech.*, *280*, 95, 1994.

Parenti, S., M. Velli, G. Poletto, S. T. Suess, and D. J. McComas, Magnetic flux tubes at 3 AU?, *Sol. Phys.*, *174*, 329, 1997.

Richter, P., and M. Scholer, On the stability of rotational discontinuities, *Geophys. Res. Lett.*, *16*, 1257, 1989.

Riley, P., C. P. Sonett, B. T. Tsurutani, A. Balogh, R. J. Forsyth, and G. W. Hoogeveen, Properties of arc-polarized Alfvén waves in the ecliptic plane: Ulysses observations, *J. Geophys. Res.*, *101*, 19,987, 1996.

Roberts, D. A., L. W. Klein, M. L. Goldstein, and W. H. Matthaeus, The nature and evolution of magnetohydrodynamic fluctuations in the solar wind: Voyager observations, *J. Geophys. Res.*, *92*, 11,021, 1987a.

Roberts, D. A., M. L. Goldstein, L. W. Klein, and W. H. Matthaeus, Origin and evolution of fluctuations in the solar wind: Helios observations and Helios-Voyager comparisons, *J. Geophys. Res.*, *92*, 12,023, 1987b.

Ruzmaikin, A., and M. A. Berger, On a source of Alfvén waves heating the solar corona, *Astron. Astrophys.*, *337*, L9, 1998.

Sakurai, T., M. Goossens, and J. V. Hollweg, Resonant behaviour of MHD waves on magnetic flux tubes, I, connection formulae at the resonant surfaces, *Sol. Phys.*, *133*, 227, 1991.

Smith, E. J., Observed properties of interplanetary rotational discontinuities, *J. Geophys. Res.*, *78*, 2088, 1973.

Spangler, S. R., Two-dimensional magnetohydrodynamics and interstellar plasma turbulence, *Astrophys. J.*, *522*, 879, 1999.

Spangler, S. R., and S. Mancuso, Radioastronomical constraints on coronal heating by high frequency Alfvén waves, *Astrophys. J.*, *530*, 491, 2000.

Terasawa T., M. Hoshino, J. Sakai, and T. Hada, Decay instability of finite-amplitude circularly polarized Alfvén waves: A numerical simulation of stimulated brillouin scattering, *J. Geophys. Res.*, *91*, 4171, 1986.

Tsurutani, B. T., and C. M. Ho, Review of discontinuities and Alfvén waves in interplanetary space: Ulysses results, *Rev. Geophys.*, 37, 517, 1999.

Tsurutani, B. T., and E. J. Smith, Interplanetary discontinuities: Temporal variations and the radial gradient from 1 to 8.5 AU, *J. Geophys. Res.*, *84*, 2773, 1979.

Tu, C.-Y., The damping of interplanetary Alfvénic fluctuations and the heating of the solar wind, *J. Geophys. Res.*, *93*, 7, 1988.

Tu, C.-Y., and E. Marsch, Two-fluid model for heating the solar corona and acceleration of the solar wind by high-frequency Alfvén waves, *Sol. Phys.*, *171*, 363, 1997.

Uberoi, C., Alfvén waves in inhomogeneous magnetic fields, *Phys. Fluids*, *15*, 1673, 1972.

Valley, G. C., Scattering of Alfvén waves by random density fluctuations, *Astrophys. J.*, *188*, 181, 1974.

Vasquez, B. J., Simulation study of the role of ion kinetics in low-frequency wave train evolution, *J. Geophys. Res.*, *100*, 1779, 1995.

Vasquez, B. J., and P. J. Cargill, The evolution of strongly modulated, low-frequency, moderate amplitude wave packets in a dispersive plasma, *Phys. Fluids B*, *5*, 42, 1993.

Vasquez, B. J., and J. V. Hollweg, Formation of arc-shaped Alfvén waves and rotational discontinuities from oblique linearly polarized wave trains, *J. Geophys. Res.*, *101*, 13,527, 1996a.

Vasquez, B. J., and J. V. Hollweg, The making of an Alfvénic fluctuation: The resolution of a second-order analysis, in *Solar Wind Eight*, edited by D. Winterhalter et al., *AIP Conf. Proc.*, *382*, 331, 1996b.

Vasquez, B. J., and J. V. Hollweg, Formation of spherically polarized Alfvén waves and imbedded rotational discontinuities from a small number of entirely oblique waves, *J. Geophys. Res.*, *103*, 335, 1998a.

Vasquez, B. J., and J. V. Hollweg, Formation of imbedded rotational discontinuities with nearly field aligned normals, *J. Geophys. Res.*, *103*, 349, 1998b.

Vasquez, B. J., and J. V. Hollweg, Formation of pressure-balanced structures and fast waves from nonlinear Alfvén waves, *J. Geophys. Res.*, *104*, 4681, 1999.

Yang, G., and J. V. Hollweg, The effects of velocity shear on the resonance absortpion of MHD surface waves: Cold plasma, *J. Geophys. Res.*, *96*, 13,807, 1991.

Bernard J. Vasquez and Joseph V. Hollweg, Space Science Center, Institute for the Study of Earth, Oceans, and Space, University of New Hampshire, Durham, NH 03824-3525. (bernie.vasquez@unh.edu)

(Received July 10, 2000; revised August 31, 2000; accepted October 12, 2000.)